# Stochastic-priority-integrated signal coordination considering connected bus operation uncertainties

Ou, Shiqi; An, Kun; Ma, Wanjing; Hegyi, Andreas; van Arem, Bart

**DOI**
10.1080/21680566.2023.2297152

**Publication date**
2023

**Document Version**
Final published version

**Published in**
Transportmetrica B

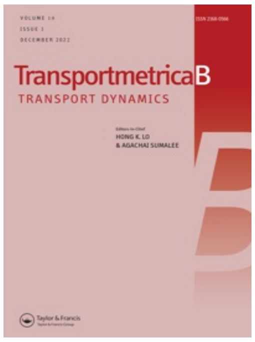

Taylor & Francis
Taylor & Francis Group

Transportmetrica B: Transport Dynamics

ISSN: (Print) (Online) Journal homepage: www.tandfonline.com/journals/ttrb20

# Stochastic-priority-integrated signal coordination considering connected bus operation uncertainties

Shiqi Ou, Kun An, Wanjing Ma, Andreas Hegyi & Bart van Arem

**To cite this article:** Shiqi Ou, Kun An, Wanjing Ma, Andreas Hegyi & Bart van Arem (2024) Stochastic-priority-integrated signal coordination considering connected bus operation uncertainties, Transportmetrica B: Transport Dynamics, 12:1, 2297152, DOI: 10.1080/21680566.2023.2297152

**To link to this article:** https://doi.org/10.1080/21680566.2023.2297152

Published online: 29 Dec 2023.

TRANSPORTMETRICA B: TRANSPORT DYNAMICS
2024, VOL. 12, NO. 1, 1–25
https://doi.org/10.1080/21680566.2023.2297152

Taylor & Francis
Taylor & Francis Group

Check for updates

# Stochastic-priority-integrated signal coordination considering connected bus operation uncertainties

Shiqi Ou[a,b], Kun An[a], Wanjing Ma [a], Andreas Hegyi[b] and Bart van Arem[b]

[a]The Key Laboratory of Road and Traffic Engineering of the Ministry of Education, Tongji University, Shanghai, People's Republic of China; [b]Department of Transport and Planning, Delft University of Technology, Delft, The Netherlands

**ABSTRACT**
Multimodal arterial signal coordination for buses and passenger vehicles can improve arterial travel smoothness and efficiency. However, uncertainty in bus operations requires signal priority at intersections, which impacts coordination and increases stop times for other traffic types. Therefore, this study proposes a stochastic priority-integrated signal coordination (SPIC) method. It includes an offline stochastic programme to determine the arterial signal coordination, i.e. cycle length and offsets, considering the stochastic signal priority, and an online mixed-integer nonlinear programme to determine the signal priority together with the bus arrival and departure times at and from stops and intersections in a connected vehicle environment. A scenario-based heuristic algorithm is proposed to solve the SPIC efficiently. Numerical studies have validated that SPIC can improve the efficiency of buses and passenger vehicles. Sensitivity analyses show that the SPIC effectively reduces delays with fluctuations in the bus travel time, dwell time, and passenger vehicle demands.

**ARTICLE HISTORY**
Received 7 July 2023
Accepted 2 November 2023

**KEYWORDS**
Arterial signal coordination; bus operation uncertainty; transit signal priority; connected bus; stochastic programme

## 1. Introduction

Arterial signal coordination is a cost-effective solution widely implemented in urban areas to allow the continuous movement of vehicles, thereby reducing stop times and delays. In densely populated areas, where public transport is a major concern, it is crucial to implement arterial signal coordination for transit and passenger vehicles to ensure efficient and reliable transit services (He, Head, and Ding 2014; Ma et al. 2019). However, uncertainty in bus operation can result in a bus missing consecutive green lights, rendering signal coordination ineffective. To address this problem, real-time signal priority based on existing signal coordination has been proposed to guarantee bus progression in the arteries (Das, Vasant Altekar, and Head 2023). However, uncertain signal priority can affect the optimality of the existing coordination plan, increasing the stop times and delays for other traffic. Moreover, only a few studies have considered the influence of bus signal priority on arterial signal coordination. Therefore, this study focuses on developing an arterial signal coordination control method that considers the impact of uncertain signal priority.

Traditional signal coordination control can be classified into two categories. The first category aims to maximise the bandwidth along the artery (Cho, Huang, and Huang 2019; Gartner et al. 1990). This

**CONTACT** Kun An kunan@tongji.edu.cn; Wanjing Ma mawanjing@tongji.edu.cn The Key Laboratory of Road and Traffic Engineering of the Ministry of Education, Tongji University, Shanghai, People's Republic of China

approach provides progression bands along an artery for vehicles to pass through consecutive intersections without stopping. However, it is less effective when high-volume traffic enters an artery or busy streets because these flows are not considered. The second category aims to optimise traffic-related indicators such as delay (Zhou, Hawkins, and Zhang 2017), capacity (Su et al. 2023), and travel time (Van De Weg et al. 2019), providing a more comprehensive representation of the overall traffic performance by considering all flows in the system.

With the increasing importance of transit vehicles, multimodal signal coordination control has gained considerable attention. Therefore, bandwidth-oriented methods that considered multiple modes, including buses and passenger vehicles, were proposed (Florek 2020; Ma et al. 2019). However, buses often have sparse and uncertain arrival times, making it difficult for them to remain within the provided progression band. Other studies proposed optimisation methods that minimised passenger delays (Chen, Cheng, and Chang 2021), passenger travel time (Estrada et al. 2016), and transit reliability levels (Chow et al. 2021). However, these deterministic methods did not account for real-time bus operations, such as uncertain travel times, resulting in unrealistic models and poor signal control in the real world.

Studies have been conducted on arterial signal control, considering uncertainties in bus operations. Arterial coordinated signal priority methods were developed with regard to the bus dwell time, travel time, and downstream progression (Liang et al. 2023; Truong et al. 2019). However, these studies focused on bus efficiency and neglected passenger vehicle efficiency. Traffic demand uncertainty was also frequently considered by building multistage stochastic programmes for coordinated signal control minimising system delays (Li et al. 2022; Li, Huang, and Lo 2018) or maximising throughput (Su et al. 2023). However, they primarily focused on avoiding overflow of passenger vehicles. Moreover, adaptive signal control methods for arteries were proposed to address uncertain bus operations using adaptive signal coordination and coordinated signal priority. Adaptive signal coordination adjusted the offsets according to real-time traffic states (Li, Huang, and Lo 2018; Xiang and Chen 2016). However, frequently adjusting the offsets may disrupt vehicle platoons on the artery. The practical benefits of adaptively and dynamically changing the signal coordination plans should be carefully evaluated. Coordinated signal priority methods were developed for region-wide intersections by considering coordination as a form of priority (Das, Vasant Altekar, and Head 2023), considering bus operating benefits at downstream intersections (Li et al. 2021; Ma et al. 2013), or restricting priority conditions according to the existing signal coordination by imposing strict progression-breaking prevention constraints (Beak, Head, and Feng 2017; Liang, Xiao, and Flötteröd 2021) or relaxed progression-breaking penalties (He, Head, and Ding 2014). However, the effectiveness of these signal priority methods is restricted by existing signal coordination plans. The signal coordination in these studies was typically predetermined and did not consider the impacts of uncertain bus signal priority at intersections. In real-world applications, adaptive signal priority may break the existing signal coordination, thereby increasing travel delays for other traffic on arteries and side streets, thus making it necessary to develop a multimodal signal coordination method that considers stochasticity in the signal priority.

Fortunately, connected vehicle (CV) technologies make it easier to implement arterial signal coordination with stochastic signal priority at intersections. In a CV environment, historical bus operational data can be collected and analysed to understand the bus travel characteristics. Despite the availability of real-time bus operational data, the signal coordination plan is more suitable for remaining unchanged for a period during which the bus operational parameters tend to be stochastic. The impact of this stochasticity on bus operation affects the signal coordination performance, thus making it necessary to include the effects of the stochastic bus operation when optimising the signal coordination plan. Moreover, real-time information on buses, such as speed and location, can be obtained using signal controllers, allowing improved signal priority efficiency (Yang, Menendez, and Guler 2019; Zeng et al. 2021). Auxiliary control methods such as speed advisory and adaptive signal control at intersections can reduce the impact of buses on signal coordination in CV environments (Hu et al. 2021; Wu et al. 2018).

System performance measures are crucial for developing signal coordination control methods. Delays are commonly used as indicators of system efficiency; however, there are limited vehicle delay estimation methods under coordinated signal control. These can be classified into the shockwave theory and residual queue effect-based approaches. By combining the shockwave theory and Bayesian networks, vehicle delay prediction methods for two adjacent intersections with coordination were developed with known vehicle arrival rates (Mohajerpoor, Saberi, and Ramezani 2017; Wang, Huang, and Lo 2020). However, they did not consider the delays caused by other traffic joining the artery from side streets. Another delay prediction method that incorporates the effects of the residual queue at downstream intersections, offsets, and stochastic traffic arrivals was proposed (Li, Huang, and Lo 2018). Similarly, a coordinated adaptive control focusing on reducing overflow based on residual queue effects was developed (Ma, An, and Lo 2016). However, these methods have high computational complexity and do not consider acceleration/deceleration delays, which reflect travel smoothness. Therefore, a delay estimation method suitable for arterial signal coordination control with stochastic bus operations and fluctuating traffic arrival profiles needs to be proposed.

Notwithstanding the abundant studies, ignoring bus operation stochasticity leads to unrealistic models and poor signal control, thus making it necessary to evaluate multimodal arterial signal coordination control considering the stochastic signal priority. A stochastic programme (SP) and a mixed-integer nonlinear programme (MINLP) are formulated to cooperatively determine the optimal cycle length, offsets, and signal priority strategies at intersections. The objective function aims to minimise the weighted bus and passenger vehicle delays. Signal priority control, bus trajectories, and passenger vehicle delays were explicitly modelled. A novel passenger vehicle delay estimation method that considers arterial signal coordination is proposed. The bus travel time, dwell time at the stops, and arrival time at the artery are stochastic parameters. This study aims to develop a stochastic priority-integrated coordination (SPIC) method for arterial signal control with the following features.

(1) Offline signal coordination: We design a signal coordination method that considers the influence of future signal priority control.
(2) Online signal priority: We provide a coordinated signal priority control method with a signal coordination background.
(3) Stochasticity consideration: We consider the stochastic signal priority because of the uncertainty in the bus travel time, dwell time, and arrival time at the artery.
(4) Connected bus guidance: We plan the bus arrival/departure times at bus stops and intersections as guidance in a CV environment.

The remainder of this paper is organised as follows. Section 2 describes this problem. Section 3 introduces the SPIC control method together with the signal priority control method. Section 4 describes the proposed solution algorithm. Section 5 discusses the numerical studies, analyses the results and tests the sensitivity of the proposed methods. Finally, Section 6 concludes the study.

## 2. Problem description

The left side of Figure 1 shows an artery with buses and passenger vehicles equipped with dedicated bus lanes. Bus stops are built where buses must stop to serve passengers. For example, the proposed method uses an artery with leftmost dedicated bus lanes. The model can also be applied to the case of the rightmost dedicated bus lanes by imposing modified phase-conflicting restrictions. The buses are connected in a CV environment equipped with roadside units for real-time communication; thus, real-time bus location, speed, and historical operational information are available as data inputs to the SPIC embedded in the roadside/central signal controller, while real-time control policies can be sent to the buses, as shown on the right side of Figure 1. The bus dwell time and travel time are considered stochastic parameters. The arrival profiles of passenger vehicles and their segment travel times are known. Arterial buses are prioritised. Real-time signal priority is enabled by green extension and green

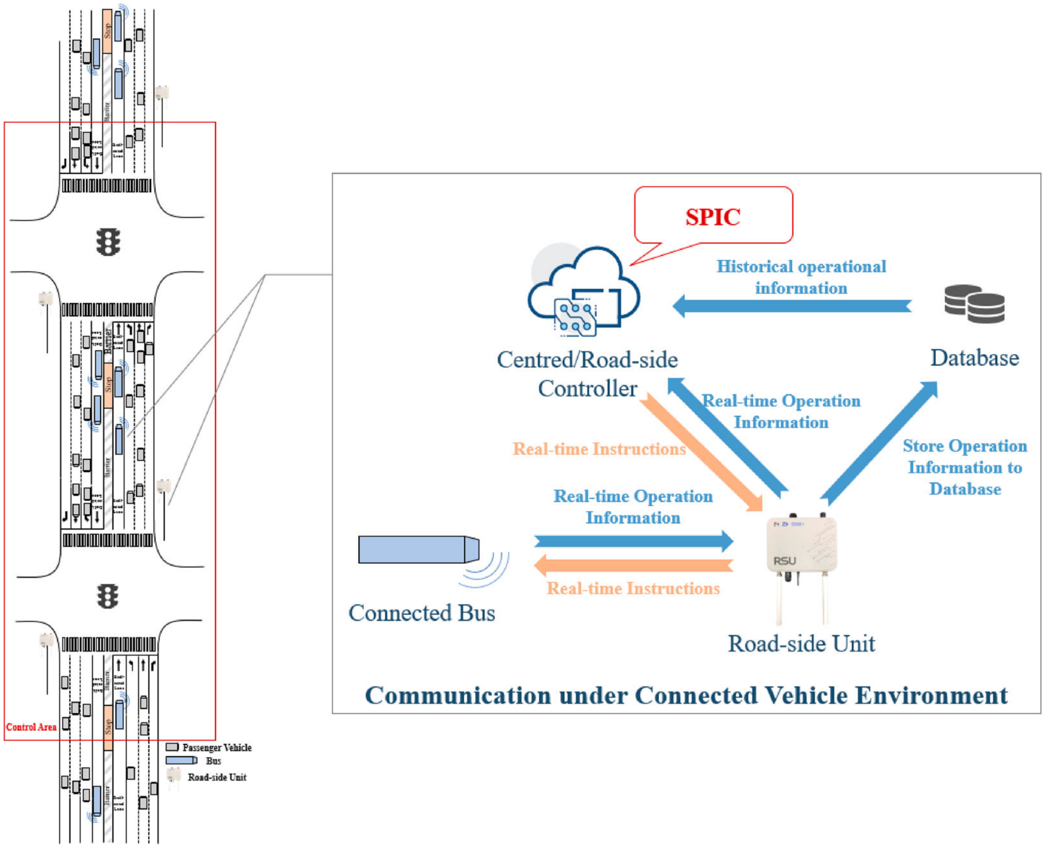


**Figure 1.** Artery with connected buses and passenger vehicles under CV environment.

advance. An existing signal control plan exists for each intersection, and the phase sequences remain the same as the existing sequences; overlapping of the non-conflicting phases is allowed. Buses and passenger vehicles with the same traffic movement share the same phase.

The task is to minimise the total delays by adjusting the uniform cycle length along the artery and the offset of each intersection considering the stochasticity of the signal priority strategies at intersections due to the stochastic bus dwell and travel times, and to design signal priority strategies at intersections to cater to time-varying bus operations. Using historical data (including passenger vehicle arrival profiles at intersections, bus travel time, dwell time, and bus arterial arrival times), existing road designs, and signal control plans, this study focuses on optimising the cycle length and offsets offline, considering the impacts of the future stochastic signal priority, and optimising the signal priority plans at intersections online, together with the bus arrival/departure times at stops and intersections with real-time bus operational information. The bus operational information is updated in real time and used to calculate the optimal signal priority plans and bus arrival/departure times at the stops and intersections. There can be several signal coordination plans for different periods of the day. The following assumptions are made to analyse the problem:

(1) The distributions of the stochastic bus dwell time and travel time over a period can be obtained from historical bus operational data (Johar, Jain, and Garg 2016). The real-time bus dwell time and bus travel time in a dedicated bus lane can be predicted accurately using the real-time bus arrival times (Bian et al. 2015; Ma et al. 2019).

(2) Each bus can plan its trajectory to reach an intersection or stop at the optimal arrival time when it is on the nearest upstream segment of the intersection.
(3) Dedicated bus lanes for buses are provided. Turning buses have to use lanes shared by passenger vehicles.

## 3. Model formulation

This section develops an SP to optimise the cycle length and offsets and an MINLP to optimise the green splits of intersections and bus arrival/departure times. The goal is to minimise the total delay over a predefined horizon $T$ for multiple signal control cycles. While the model formulation for one cycle is provided, it applies to all cycles. Uncertainties in the bus travel time, dwell time, and arterial arrival time are addressed using sample-average approximation (SAA). The objective function $J(x) = E[J(x, \xi)]$, where $x$ denotes the decision variable and $\xi$ is a stochastic element with a known distribution that does not depend on $x$. SAA uses fixed samples $\xi_1, \xi_2, \ldots, \xi_n$ that follow the same and known distribution as $\xi$ to appropriate $J(x)$ to ensure that deterministic optimisation algorithms can be applied to solve the problem $\min\limits_{x \in D} J_n(x)$, where $D$ denotes the feasible domains of $x$. This study uses a sample index $s \in S$, with fixed samples randomly drawn for the bus travel time, dwell time, and arrival time. The sampling distributions of the stochastic parameters should be validated using the historical bus operational data of the artery. Table 1 lists the notations used in this study.

### 3.1. Constraints

Constraints dealing with signal control (including signal coordination variable domains and signal priority control rules), bus trajectories, and passenger vehicle delays are established in this section.

#### 3.1.1. Signal coordination variable domains

The uniform cycle length $C$ for the intersections of the arteries is bounded by the minimal and maximal lengths (Eq. (1)). The synchronisation of the signal timing along the artery in the two directions is guaranteed by the relative offset $O_i$ of each intersection, which is the time that the signal control cycle of intersection $i$ starts later than that of intersection 1. The relative offsets are bounded between zero and one represented by the fraction of the cycle (Eq. (2)). In all samples, the cycle length and offsets

**Table 1.** Notations.

| Notations | Variable description | unit |
|---|---|---|
| **Sets and parameters** | | |
| $\Omega$ | Set of intersections on the artery, $\Omega = \{1, 2, \ldots, I\}$. | / |
| $P_i$ | Set of phases at intersection $i$, $P_i = \{1, \ldots, 8\}, i \in \Omega$. | / |
| $P_i^c/P_i^d$ | Set of phases for the artery/the side street approaches at intersection $i$. | / |
| $P_i^u(P_i^l)$ | Set of phases of the outbound (inbound) ring at intersection $i$. | / |
| $S = \{s\}$ | Set of samples. Each sample has given values of bus travel time, dwell times at stop, and arrival time at the artery. | / |
| $Y_s\bar{Y}_s$ | Set of outbound (inbound) buses in sample $s$, $s \in S$. | / |
| $a_{s,y}^b(\bar{a}_{s,y}^b)$ | Outbound (inbound) arrival time at the artery of bus $y$ in sample $s$, $y \in Y_s(\bar{Y}_S)$ | second |
| $\tilde{d}^a$ | Passenger vehicle deceleration/acceleration delay caused by stop. | second |
| $e_i$ | Sum of yellow time and all red time for each phase at intersection $i$. | second |
| $\tilde{G}_{i,p}^r/\tilde{G}_{i,p}^e$ | Original start/end point of phase $p$ at intersection $i$, $p \in P_i$. | fraction of cycle |
| $g_{i,p}$ | Original phase duration of phase $p$ at intersection $i$, including green time, yellow time, and all red time. | fraction of cycle |
| $\check{g}_{i,p}$ | Minimal phase duration of phase $p$ at intersection $i$. | second |
| $\hat{g}_i^x$ | Maximal outbound green extension duration at intersection $i$. | second |
| $\hat{g}_i^v$ | Maximal outbound green advance duration at intersection $i$. | second |
| $\tilde{h}_{s,i}^r/\tilde{h}_{s,i}^e$ | Cycle starting time of the next cycle/cycle end time of the previous cycle at intersection $i$. | fraction of cycle |

(*continued*).

**Table 1.** Continued.

| Notations | Variable description | unit |
|---|---|---|
| $\tilde{q}^{a}_{i,m}(t)$ | Number of arrival passenger vehicles of movement $m$ at intersection $i$ at time step $t$, $t \in Z \cap \{x \mid x < T\}$, $m \in \{1, \ldots, 12\}$, representing movements of a left turn (LT), going through (GT), and a right turn (RT) from the west approach, LT, GT, and RT from the south approach, LT, GT, and RT from the east approach, and LT, GT, and RT from the north approach, respectively. | pcu/ second |
| $q^{u}_{i,p}$ | Saturated departure rate of phase $p$ at intersection $i$. | pcu/ second |
| $t^{a}_{i}(\bar{t}^{a}_{i})$ | Travel time of outbound (inbound) passenger vehicles between intersection $i$ and intersection $i+1, i \in \Omega, i \neq I$. | second |
| $t^{b}_{s,i,y}(\bar{t}^{b}_{s,i,\bar{y}})$ | Travel time (excluding stop dwell time) of outbound (inbound) bus $y$ along the upstream road segment towards intersection $i$ in sample $s$. | second |
| $t^{safe}$ | Safe headway between a pair of buses. | second |
| $u^{b}_{s,i,y}(\bar{u}^{b}_{s,i,\bar{y}})$ | Dwell time of outbound (inbound) bus $y$ at the bus stop along the downstream segment of intersection $i$ in sample $s$. | second |
| $\gamma_{i,p,m}$ | 1, if phase $p$ in intersection $i$ allows movement $m$ to pass, where $m \in \{1, \ldots, 12\}$; 0, otherwise. | / |
| **Decision variables** | | |
| $C$ | Uniform cycle length. | second |
| $O_i$ | Difference between the start time of the first phase of intersection $i$ and that of intersection 1, namely the relative offsets, $i \in \Omega$. | fraction of cycle |
| $\bar{\bar{g}}_{s,i,p}$ | Duration of phase $p$ at intersection $i$ in sample $s$, $s \in S, i \in \Omega, p \in P_i$. | fraction of cycle |
| **Auxiliary variables** | | |
| $\mathbb{D}^{a}_{s}/\mathbb{D}^{b}_{s}$ | Total delay of passenger vehicles/buses in sample $s$. | pcu· second |
| $D^{a}_{s,i,p}$ | Delay of passenger vehicles of phase $p$ at intersection $i$ in sample $s$. | pcu/ second |
| $d^{b}_{s,i,y}(\bar{d}^{b}_{s,i,y})$ | Stopping duration at intersection $i$ of outbound (inbound) bus $y$ in sample $s$. | fraction of cycle |
| $G^{r}_{s,i}\bar{G}^{r}_{s,i}/G^{e}_{s,i}(\bar{G}^{e}_{s,i})$ | Start/End point of the priority period in the outbound (inbound) direction at intersection $i$ in sample $s$. | fraction of cycle |
| $h^{r}_{s,i}(\bar{h}^{r}_{s,i})/\ h^{e}_{s,i}(\bar{h}^{e}_{s,i})$ | Cycle start/end point in the outbound (inbound) direction at intersection $i$ in sample $s$. | fraction of cycle |
| $l_{s,i,p}(t)$ | Passenger vehicle queue length (the number of vehicles) of phase $p$ at time step $t$ at intersection $i$ in sample $s$. | pcu |
| $N^{s}_{s,i,p}(t)$ | Number of passenger vehicles that stop at intersection $i$ during phase $p$ at time step $t$ in sample $s$. | pcu |
| $q^{a}_{s,i,p}(t)$ | Number of arrival passenger vehicles of phase $p$ at time step $t$ at intersection $i$ in sample $s$. | pcu/ second |
| $q^{d}_{s,i,p}(t)$ | Number of departure passenger vehicles of phase $p$ at time step $t$ at intersection $i$ in sample $s$. | pcu/ second |
| $w^{b}_{s,i,y}(\bar{w}^{b}_{s,i,y})$ | Difference between the departure time of outbound (inbound) bus $y$ in sample $s$ and the start time of phase 1 at intersection $i$. | fraction of cycle |
| $\alpha^{1}_{s,i}(\bar{\alpha}^{1}_{s,i})$ | 0, if signal priority is adopted in the outbound (inbound) direction at intersection $i$ in sample $s$; 1, otherwise. | / |
| $\alpha^{2}_{s,i}(\bar{\alpha}^{2}_{s,i})$ | Binary variables related to signal priority type in the outbound (inbound) direction at intersection $i$ in sample $s$. | / |
| $\beta_{s,i,y}(\bar{\beta}_{s,i,y})$ | 1, if bus $y$ leaves intersection $i$ in sample $s$ during the original green time; 0, if bus $y$ leaves intersection $i$ in sample $s$ in the outbound (inbound) direction during the signal priority period. | / |
| $\delta^{b}_{s,i,y}(\bar{\delta}^{b}_{s,i,y})$ | 1, if $G^{r}_{s,i}$ and $G^{e}_{s,i}$ are non-positive (when green advance is conducted); 0, otherwise. | / |
| $\eta^{b}_{s,i,y}(\bar{\eta}^{b}_{s,i,y})$ | Number of cycles that outbound (inbound) bus $y$ takes to reach intersection $i$ from its upstream intersection in sample $s$. | / |
| $\varpi_{s,i,y_1,y_2}$ | 1, if bus $y_2$ leaves intersection $i$ earlier than bus $y_1$ in sample $s$; 0, otherwise. | / |
| $\omega^{1}_{s,i,p}(t)$ | 1, if there are queues of passenger vehicles of phase $p$ at time step $t$ at intersection $i$ in sample $s$; 0, otherwise. | / |
| $\omega^{2}_{s,i,p}(t)$ | 1, if the discharging rate for passenger vehicles of phase $p$ is zero at time step $t$ at intersection $i$ in sample $s$; 0, if the discharging rate is saturated. | / |

remain unchanged.

$$\check{C} \leq C \leq \hat{C} \tag{1}$$

$$0 \leq O_i < 1, \forall i \in \Omega \tag{2}$$

where $\check{C}$ and $\hat{C}$ denote the minimal and maximal cycle lengths; and $\Omega$ denotes the set of intersections along the artery.

Figure 2 shows the standard NEMA ring barrier structure used in this study. The blue arrow indicates the reference time for the offsets. The structure includes two barrier groups, separating east–west from

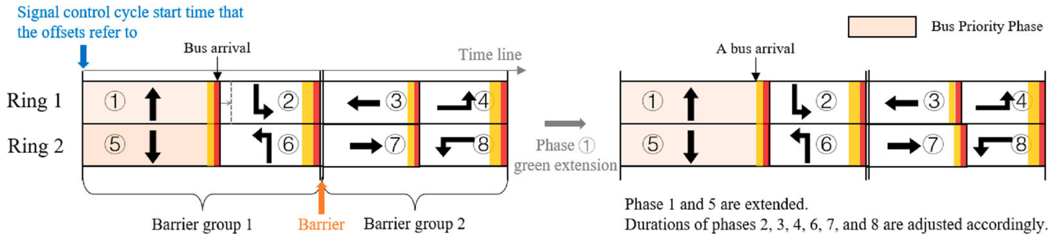


**Figure 2.** NEMA ring barrier structure.

north–south movements, starting and ending simultaneously in both rings. Each phase follows a predefined sequence, which remains unchanged in this study, indexed from one to eight. The prioritised phases located in barrier group 1 are phases 1 and 5, phases 1 and 6, phase 2 and 5, or phases 2 and 6. Figure 2 illustrates the signal plans before and after the green extension in Phase 1. With the green extension, the phase durations are adjusted to minimise the total delay. Phase 5 is extended to prevent overlap, with the durations of the other phases reduced. The optimisation yields an overlap of Phases 7 and 4.

### 3.1.2. *Signal priority control rules*

(1) Signal priority rules

At any intersection along the artery, two types of signal priority methods, green extension, and green advance, can be adopted according to the bus arrivals. However, these processes cannot be conducted simultaneously at an intersection. Two auxiliary binary variables $\alpha_{s,i}^1$ and $\alpha_{s,i}^2$ are introduced to represent the three signal priority control situations for modelling and the meaning of their values are shown in Figure 3. Notably, the inbound variables with an overbar ($\bar{\alpha}_{s,i}^1$ and $\bar{\alpha}_{s,i}^2$) have a similar meaning as those ($\alpha_{s,i}^1$ and $\alpha_{s,i}^2$) of the outbound direction. The signal priority plans differ from each other in different samples, indexed by $s \in S$.

In the following section, we use the outbound direction constraints as an example. The corresponding constraints for the inbound direction can be obtained by simply replacing the related variables such as replacing $\alpha_{s,i}^1$ by $\bar{\alpha}_{s,i}^1$, etc. In each signal priority situation, the priority green time denotes the extra green time given to buses compared with the original signal timing. The original signal timing

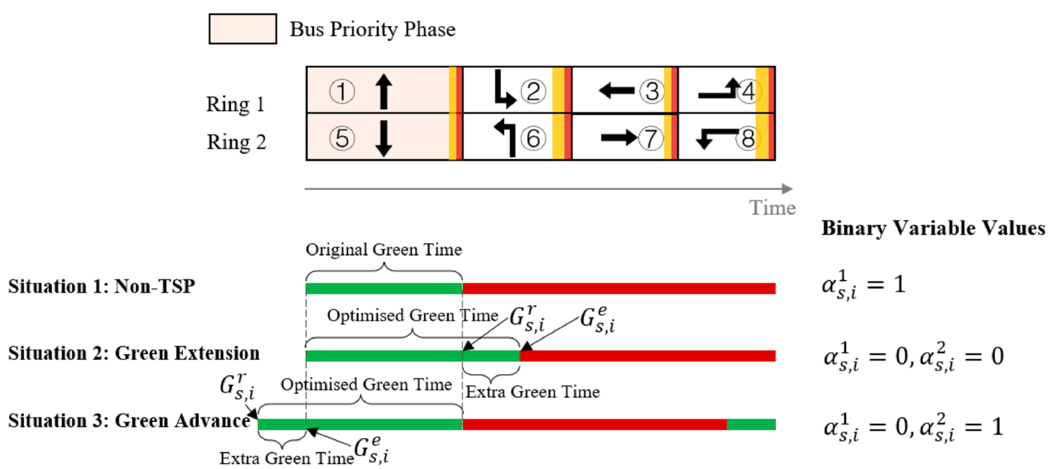


**Figure 3.** Signal priority situations.

refers to the existing signal control plan used in the real world. The fractions of the cycle $G^r_{s,i}$ and $G^e_{s,i}$ denote the start and end of the priority green period, respectively, as shown in Figure 3. $G^r_{s,i}$ and $G^e_{s,i}$ are constrained according to the priority rules of the three situations. If no signal priority control is conducted ($\alpha^1_{s,i} = 1$), then Eqs. (3)–(4) hold. This indicates $G^r_{s,i} = G^e_{s,i} = \tilde{G}^r_{i,p^a_i}$, which means zero priority time:

$$-(1-\alpha^1_{s,i})M + \tilde{G}^r_{i,p^a_i} \le G^r_{s,i} \le \tilde{G}^r_{i,p^a_i} + (1-\alpha^1_{s,i})M, \forall i \in \Omega; \forall s \in S \tag{3}$$

$$-(1-\alpha^1_{s,i})M + \tilde{G}^r_{i,p^a_i} \le G^e_{s,i} \le \tilde{G}^r_{i,p^a_i} + (1-\alpha^1_{s,i})M, \forall i \in \Omega; \forall s \in S \tag{4}$$

where M is a sufficiently large number; and $\tilde{G}^r_{i,p}$ denotes the fraction of cycle representing the original starting point of phase $p$. The same constraints are established for the inbound direction.

*Remark*: The design of the extra priority green period (rather than adjusting the durations of the existing phases) enables the model to include phase insertion for future extensions.

In the green extension situation ($\alpha^1_{s,i} = 0, \alpha^2_{s,i} = 0$), $G^r_{s,i}$ should be the end of the original green time (Eq. (5)). It should be noted that $\tilde{G}^e_{i,p^a_i}$ denotes the original endpoint of phase $p^a_i$ including the yellow time and all red times $e_i$, but the green extension should be conducted exactly at the end of the green time. Therefore, the start of the green extension $G^r_{s,i}$ should be the end of the prioritised phase minus the yellow time and all red times, $\tilde{G}^e_{i,p^a_i} - e_i/C$. In addition, $G^e_{s,i}$ should be bounded by the minimal and maximal green extension times summed up with $G^r_{s,i}$ (Eq.(6)). Similarly, in the green advance situation ($\alpha^1_{s,i} = 0$ and $\alpha^2_{s,i} = 1$), $G^e_{s,i}$ should be the start of the prioritised phase (Eq. (7)), and $G^r_{s,i}$ should be bounded by the minimum and maximum green advance times (Eq. (8)).

$$-\alpha^1_{s,i}M - \alpha^2_{s,i}M + \tilde{G}^e_{i,p^a_i} - \frac{e_i}{C} \le G^r_{s,i} \le \tilde{G}^e_{i,p^a_i} - \frac{e_i}{C} + \alpha^1_{s,i}M + \alpha^2_{s,i}M, \forall i \in \Omega; \forall s \in S \tag{5}$$

$$-\alpha^1_{s,i}M - \alpha^2_{s,i}M + G^r_{s,i} \le G^e_{s,i} \le G^r_{s,i} + \hat{g}^x_i/C + \alpha^1_{s,i}M + \alpha^2_{s,i}M, \forall i \in \Omega; \forall s \in S \tag{6}$$

$$-\alpha^1_{s,i}M - (1-\alpha^2_{s,i})M + \tilde{G}^r_{i,p^a_i} \le G^e_{s,i} \le \tilde{G}^r_{i,p^a_i} + \alpha^1_{s,i}M + (1-\alpha^2_{s,i})M, \forall i \in \Omega; \forall s \in S \tag{7}$$

$$-\alpha^1_{s,i}M - (1-\alpha^2_{s,i})M + G^e_{s,i} - \frac{\hat{g}^v_i}{C} \le G^r_{s,i} \le G^e_{s,i} + \alpha^1_{s,i}M + (1-\alpha^2_{s,i})M, \forall i \in \Omega; \forall s \in S \tag{8}$$

where $e_i$ denotes the sum of the yellow time and all red time for each phase at intersection $i$ in seconds; $\hat{g}^x_i$ denotes the maximal green extension times; $\hat{g}^v_i$ denotes the maximal green advance times; and $\tilde{G}^e_{i,p^a_i}$ denotes the fraction of the cycle representing the original endpoint of phase $p$.

As the prioritised phase is Phases 1 or 5, the cycle starts earlier if the green advance priority is conducted. Thus, to consider the effects on and of the previous cycle, variables denoting the relative cycle start times, $h^r_{s,i}$, are introduced. It is zero if the cycle start time does not change and negative if the cycle starts earlier. Its absolute value denotes the change in the cycle start time. Therefore, $h^r_{s,i} = -(G^e_{s,i} - G^r_{s,i})$ if the green advance priority is conducted ($\alpha^1_{s,i} = 0$ and $\alpha^2_{s,i} = 1$), as shown in Eq. (9). Otherwise, $h^r_{s,i} = 0$, as expressed in Eqs. (10)–(11).

$$\begin{aligned} -\alpha^1_{s,i}M - (1-\alpha^2_{s,i})M - (G^e_{s,i} - G^r_{s,i}) \le h^r_{s,i} \le \\ -(G^e_{s,i} - G^r_{s,i}) + \alpha^1_{s,i}M + (1-\alpha^2_{s,i})M, \forall i \in \Omega; \forall s \in S \end{aligned} \tag{9}$$

$$-(1-\alpha^1_{s,i})M \le h^r_{s,i} \le (1-\alpha^1_{s,i})M, \forall i \in \Omega; \forall s \in S \tag{10}$$

$$-\alpha^2_{s,i}M \le h^r_{s,i} \le \alpha^2_{s,i}M, \forall i \in \Omega; \forall s \in S \tag{11}$$

(2) Phase splits

The splits of each phase may change accordingly with the signal priority; however, they are subject to barrier constraints and physical restrictions. If no signal priority is conducted ($\alpha^1_{s,i} = 1$), $\overline{\overline{g}}_{s,i,p} = g_{i,p}$, which means the phase time equals the corresponding original phase time, as shown in Eq. (12). The minimal green time restriction is given by Eq. (13). Changes in the phase durations due to the signal priority must be within the allowable proportion (Eq. (14)). The phases in different barrier groups cannot overlap (Eq. (15)). The phase overlap in the north–south movement barrier group is restricted (Eq. (16)) because the through-going and left-turn movements must be separated because of the leftmost through-going dedicated bus lanes.

$$-(1-\alpha^1_{s,i})M + g_{i,p} \le \overline{\overline{g}}_{s,i,p} \le g_{i,p} + (1-\alpha^1_{s,i})M, p \in P^u_i; \forall i \in \Omega; \forall s \in S \tag{12}$$

$$\overline{\overline{g}}_{s,i,p} \ge \check{g}_{i,p}/C, p \in P^u_i; \forall i \in \Omega; \forall s \in S \tag{13}$$

$$-\varphi \le \frac{\overline{\overline{g}}_{s,i,p} - g_{i,p}}{g_{i,p}} \le \varphi, p \in P^u_i; \forall i \in \Omega; \forall s \in S \tag{14}$$

$$\sum_{p=1}^{2} \overline{\overline{g}}_{s,i,p} = \sum_{p=5}^{6} \overline{\overline{g}}_{s,i,p}, \forall i \in \Omega; \forall s \in S \tag{15}$$

$$\overline{\overline{g}}_{s,i,1} = \overline{\overline{g}}_{s,i,5}, \forall i \in \Omega; \forall s \in S \tag{16}$$

where $g_{i,p}$ and $\overline{\overline{g}}_{s,i,p}$ denote the original and the optimal phase splits of phase $p$ at intersection $i$, including the green time, yellow time, and all red time; $\check{g}_{i,p}$ denotes the minimal phase length of phase $p$; $\varphi$ denotes the maximal proportion that the phase duration can be shifted because of the signal priority. The minimal green time $\check{g}_{i,p}$ is determined by the minimum pedestrian crossing time, which is related to the crossing distance and the pedestrian walking speed.

Optimal green splits should be adjusted according to the signal priority control. When the green extension or green advance is conducted ($\alpha^1_{s,i} = 0$), the split of the prioritised phase $\overline{\overline{g}}_{s,i,p}$ is its original splits $g_{i,p}$ in addition to the priority period $G^e_{s,i} - G^r_{s,i}$ (Eq. (17)). Other green split durations should be consistent with the start time of the priority time $G^r_{s,i}$. When the green extension is applied ($\alpha^1_{s,i} = 0$ and $\alpha^2_{s,i} = 0$), $\overline{\overline{g}}_{s,i,1} - e_i/C = G^e_{s,i}$, which indicates that the priority phase green time ends at the end time of the extra priority period (Eq. (18)).

$$-\alpha^1_{s,i}M + g_{i,p} + G^e_{s,i} - G^r_{s,i} \le \overline{\overline{g}}_{s,i,p} \le g_{i,p} + G^e_{s,i} - G^r_{s,i} + \alpha^1_{s,i}M, p = 1,5; \forall i \in \Omega; \forall s \in S \tag{17}$$

$$-\alpha^1_{s,i}M - \alpha^2_{s,i}M + G^e_{s,i} \le \overline{\overline{g}}_{s,i,1} - e_i/C \le G^e_{s,i} + \alpha^1_{s,i}M + \alpha^2_{s,i}M, \forall i \in \Omega; \forall s \in S \tag{18}$$

The cycle length may change because of the green advance priority. Consequently, the sum of the phase durations should consider the cycle start time $h^r_{s,i}$ and cycle end time $h^e_{s,i}$, as shown in Eq. (19). In addition, the cycle end time $h^e_{s,i}$ and start time of the next cycle $\tilde{h}^r_{s,i}$ should be consistent, as shown in Eq. (20).

$$\sum_{p=p'}^{p'+3} \overline{\overline{g}}_{s,i,p} = 1 - h^r_{s,i} + h^e_{s,i}, p' = 1; \forall i \in \Omega; \forall s \in S \tag{19}$$

$$h_{s,i}^{e} = \tilde{h}_{s,i}^{r} \tag{20}$$

where $\tilde{h}_{s,i}^{r}$ is an input parameter denoting the start time of the next cycle. $\tilde{h}_{s,i}^{r} = 0$ if the cycle start time does not change; and $\tilde{h}_{s,i}^{r}$ is negative if the cycle starts earlier. Notably, when the optimisation horizon is of several cycles, $\tilde{h}_{s,i}^{r}$ is the variable linking successive cycles.

*Remark*: Eqs. (17)–(20) are constructed when the prioritised phases are Phases 1 or 5. In other cases where the prioritised phases are Phases 2 or 6, these constraints can be easily adjusted by changing the start and end times of the prioritised phase and removing the cycle start time adjustment.

The signal priority can only be accommodated for passing buses. A binary variable $\beta_{s,i,y}$ is introduced. $\beta_{s,i,y} = 1$ if bus $y$ leaves intersection $i$ during the original green time in sample $s$; otherwise, $\beta_{s,i,y} = 0$. If signal priority is conducted ($\alpha_{s,i}^{1} = 0$), at least one bus should pass through the intersection during the priority time ($\beta_{s,i,y} = 0$), as shown in Eq. (21).

$$\alpha_{s,i}^{1} M + \sum_{y \in Y} (1 - \beta_{s,i,y}) \geq 1, \forall i \in \Omega; \forall s \in S \tag{21}$$

### *3.1.3. Bus trajectories*

(1) Arrivals at downstream intersections

As shown in Figure 4, the time at which the bus crosses the stop line of intersection $i+1$ equals the time at which it crosses its upstream intersection $i$ plus the travel time on the road segment $t_{s,i,y}^{b}$, the dwell time at the stop $u_{s,i,y}^{b}$, and the waiting time at intersection $i+1$, $d_{s,i+1,y}^{b}$, (Eqs. (22)–(23)). Relative offsets $O_i$ and $O_{i+1}$ should also be added for time synchronisation. It should be noted that the bus-turning directions do not affect Eqs. (22)–(23) but affect the original start and end points of the prioritised $\tilde{G}_{i,p_i^a}^{r}$ and $\tilde{G}_{i,p_i^a}^{e}$. Moreover, the stop-line crossing time of the first intersection on the artery in both directions should be the bus arrival time summed up with the waiting time, as expressed in

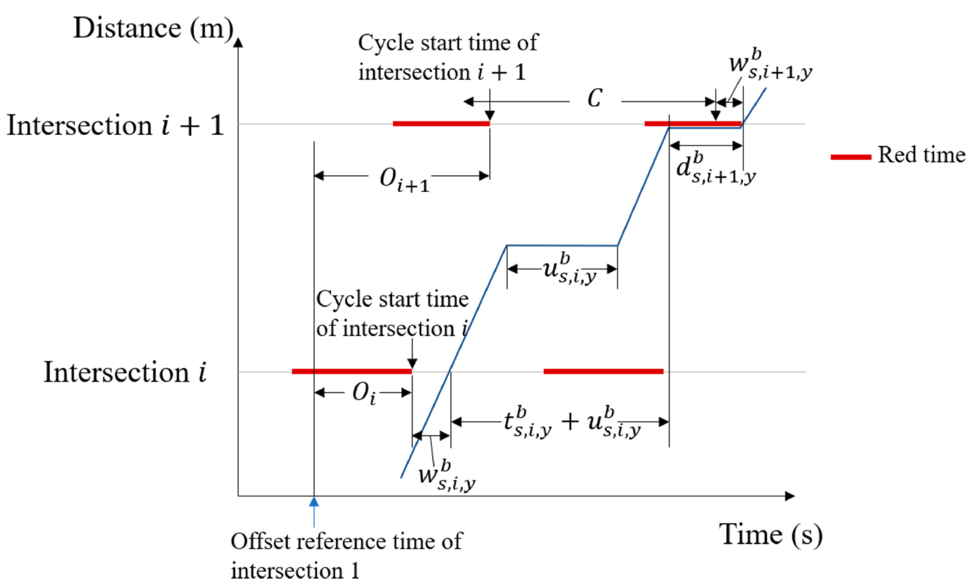


**Figure 4.** Bus trajectories between adjacent intersections.

Eq. (24).

$$0 \leq w^b_{s,i,y} < 1, \forall i \in \Omega; \forall s \in S; \forall y \in Y_s \tag{22}$$

$$O_i + w^b_{s,i,y} + t^b_{s,i,y}/C + u^b_{s,i,y}/C + d^b_{s,i+1,y} = O_{i+1} + w^b_{s,i+1,y} + \eta^b_{s,i+1,y}, \forall i \in \Omega, i \neq I; \forall s \in S; \forall y \in Y_s \tag{23}$$

$$a^b_{s,y}/C + d^b_{s,1,y} = w^b_{s,1,y} + \eta^b_{s,1,y}, \forall s \in S; \forall y \in Y_s \tag{24}$$

where $w^b_{s,i,y}$ denotes the difference between the departure time of bus $y$ and the start time of the traffic cycle that the bus crosses the stop line of intersection $i$ in sample $s$, with a unit of fractions of the cycle; $t^b_{s,i,y}$ and $u^b_{s,i,y}$ denote the travel time and dwell time of bus $y$ of the upstream segment towards intersection $i$ in seconds; $a^b_{s,y}$ denotes the arrival time at the first intersection of the artery of bus $y$ in sample $s$; $d^b_{s,i,y}$ denotes the stopping duration at intersection $i$ in sample $s$ in the form of fractions of the cycle; $\eta^b_{s,1,y}$ is an integer variable, denoting the number of cycles that bus $y$ takes to reach intersection $i$ from its upstream intersection in sample $s$; $Y_s$ denotes the set of the outbound buses on the artery. The model follows the first-come-first-serve and first-finish-first-leave rules at the bus stops.

(2) Departures from intersections

Bus $y$ crossing the stop line of intersection $i$ in sample $s$, which is denoted by $w^b_{s,i,y}$, can occur during the original green time or priority time. Eqs. (25)–(28) describe the bus passing situations. For the no signal priority case ($\alpha^1_{s,i} = 1$), Eq. (25) applies, limiting the bus passage to the original green time. Constraints without equal signs make the feasible domain of the problem an open set that potentially lacks an optimal solution. Therefore, a small $\epsilon$ is used to transform $<$ to the $\leq$ sign. When signal priority is conducted ($\alpha^1_{s,i} = 0$) and $\beta_{s,i,y} = 0$, bus $y$ passes intersection $i$ during the extra priority period, which means $G^r_{s,i} + \delta^b_{s,i,y} \leq w^b_{s,i,y} < G^e_{s,i} + \delta^b_{s,i,y}$ as shown in Eq. (26). $\delta^b_{s,i,y}$ is a binary variable for model feasibility. It is one when $G^r_{s,i}$ and $G^e_{s,i}$ are non-positive (when a green advance is conducted); otherwise, it is zero. Eq. (27) describes the situation when the green extension is in effect ($\alpha^1_{s,i} = \alpha^2_{s,i} = 0$) when $\beta_{s,i,y} = 1$. In this situation, bus $y$ passes intersection $i$ during the original green time (between the original green start time $\tilde{G}^r_{i,p^a_i}$ and green extension start time $G^r_{s,i}$). Similarly, in Eq. (28), when green advance occurs ($\alpha^1_{s,i} = 0$ and $\alpha^2_{s,i} = 1$) and $\beta_{s,i,y} = 1$, the bus departure time $w^b_{s,i,y}$ falls within the original green time (between the green advance end time $G^e_{s,i}$ and original green end time $\tilde{G}^e_{i,p^a_i}$). Buses must leave the intersection with a headway greater than the safe headway $t^{safe}$. Hence, the headway between buses $y_1$ and $y_2$, $w^b_{s,i,y_1} - w^b_{s,i,y_2}$, must either be larger than $t^{safe}$ ($\varpi_{s,i,y_1,y_2} = 1$, Eq. (29)), or less than $-t^{safe}$ ($\varpi_{s,i,y_1,y_2} = 0$, Eq. (30)). The model adheres to the first-come-first-serve rule at intersections, guaranteeing a safe headway between any pair of buses and thus preventing hindrances or collisions.

$$-(1-\alpha^1_{s,i})M + \tilde{G}^r_{i,p^a_i} \leq w^b_{s,i,y} \leq \tilde{G}^e_{i,p^a_i} - \epsilon + (1-\alpha^1_{s,i})M, \forall i \in \Omega; \forall s \in S; \forall y \in Y_s \tag{25}$$

$$-\beta_{s,i,y}M - \alpha^1_{s,i}M + G^r_{s,i} + \delta^b_{s,i,y} \leq w^b_{s,i,y} \leq G^e_{s,i} - \epsilon + \delta^b_{s,i,y} + \beta_{s,i,y}M + \alpha^1_{s,i}M, \forall i \in \Omega; \forall s \in S; \forall y \in Y_s \tag{26}$$

$$\begin{aligned} &-(1-\beta_{s,i,y})M - \alpha^1_{s,i}M - \alpha^2_{s,i}M + \tilde{G}^r_{i,p^a_i} \leq w^b_{s,i,y} \\ &\quad \leq G^r_{s,i} - \epsilon + (1-\beta_{s,i,y})M + \alpha^1_{s,i}M + \alpha^2_{s,i}M, \forall i \in \Omega; \forall s \in S; \forall y \in Y_s \end{aligned} \tag{27}$$

$$\begin{aligned} &-(1-\beta_{s,i,y})M - \alpha^1_{s,i}M - (1-\alpha^2_{s,i})M + G^e_{s,i} \leq w^b_{s,i,y} \\ &\quad \leq \tilde{G}^e_{i,p^a_i} - \epsilon + (1-\beta_{s,i,y})M + \alpha^1_{s,i}M + (1-\alpha^2_{s,i})M, \forall i \in \Omega; \forall s \in S; \forall y \in Y_s \end{aligned} \tag{28}$$

$$w^b_{s,i,y_1} - w^b_{s,i,y_2} \geq \frac{t^{safe}}{C} - (1 - \varpi_{s,i,y_1,y_2})M, \forall i \in \Omega; \forall s \in S; \forall y_1, y_2 \in Y_s, y_1 \neq y_2 \tag{29}$$

$$w^b_{s,i,y_1} - w^b_{s,i,y_2} \leq \frac{t^{safe}}{C} - \epsilon + \varpi_{s,i,y_1,y_2}M, \forall i \in \Omega; \forall s \in S; \forall y_1, y_2 \in Y_s, y_1 \neq y_2 \tag{30}$$

(3) Bus delays

The total bus delay in sample $s$, $\mathbb{D}^b_s$, can be calculated by summing the stop delays $d^b_{s,i,y}$ of buses at the intersections:

$$\mathbb{D}^b_s = \sum_{y \in Y_s} \sum_i (d^b_{s,i,y}C) + \sum_{\bar{y} \in \bar{Y}_s} \sum_i (\bar{d}^b_{s,i,\bar{y}}C) \tag{31}$$

### 3.1.4. Passenger vehicle delays

Passenger vehicle delays are calculated using cumulative arrivals, departures, and queue evolution according to Ma, Li, and Yu (2022). In this study, stop delays as well as deceleration/acceleration delays are summed at every time step. By including the deceleration/acceleration delays, the vehicle stop times are also minimised to further improve the travel smoothness of passenger vehicles. The stop delay is calculated as the queue length (number of vehicles) multiplied by the time step length. The deceleration/acceleration delays are computed by multiplying the number of stopping vehicles $N^{stop}_{s,i,p}(t)$, by a constant deceleration/acceleration delay value $\tilde{d}^a$ in Eq. (32). The queue lengths $l_{s,i,p}(t)$ evolution over time in Eqs. (33)–(34) is from Ma, Li, and Yu (2022). The time $t$ is discrete and the time step $\Delta t$ are integers.

$$D^a_{s,i,p} = \sum_{t=0}^{T-1} (l_{s,i,p}(t)\Delta t + N^{stop}_{s,i,p}(t)\tilde{d}^a), \forall i \in \Omega; \forall p \in P_i; \forall s \in S \tag{32}$$

$$l_{s,i,p}(t) = l_{s,i,p}(t-1) + q^a_{s,i,p}(t)\Delta t - q^d_{s,i,p}(t)\Delta t,\ t = 1, \ldots, T-1; \forall i \in \Omega; \forall p \in P_i; \forall s \in S \tag{33}$$

$$l_{s,i,p}(0) = l^0_{s,i,p} + q^a_{s,i,p}(0) - q^d_{s,i,p}(0), \forall i \in \Omega; \forall p \in P_i; \forall s \in S \tag{34}$$

where $D^a_{s,i,p}$ denotes the total passenger vehicle delay of phase $p$ at intersection $i$; $q^a_{s,i,p}(t)/q^d_{s,i,p}(t)$ denotes the number of arrival/departure passenger vehicles of phase $p$ at intersection $i$ at time step $t$; and $l^0_{s,i,p}$ denotes the initial queue length of phase $p$ at intersection $i$ at the start time of the control horizon.

To calculate the deceleration/acceleration delay, the number of vehicles stopping at each time step must be derived. Three situations are shown in Figure 5. The presence of a queue at intersection $i$ at time step $t$ is indicated by a binary variable $\omega^1_{s,i,p}(t)$. Similarly, a binary variable $\omega^2_{s,i,p}(t)$ describes the two discharge scenarios (either zero or saturated departures) when queues are present ($\omega^1_{s,i,p}(t) = 1$). If queues exist at time step $t$, then Eqs. (35)—(36) hold ($\omega^1_{s,i,p}(t) = 1$) with the number of departure passenger vehicle $q^d_{s,i,p}(t)$ being zero in situation 1 or saturated in situation 2. Otherwise ($\omega^1_{s,i,p}(t) = 0$, Eq. (37)), the passenger vehicle departure is unsaturated in situation 3. When a queue exists at time step $t$, all arriving vehicles at time step $t$ stop to join the queue, making $N^{stop}_{s,i,p}(t)$ equal to the number of arrival vehicles $q^a_{s,i,p}(t)\Delta t$, (Eq. (38)). Otherwise, $N^{stop}_{s,i,p}(t)$ are zero, (Eq. (39)).

$$q^d_{s,i,p}(t) \leq (1 - \omega^1_{s,i,p}(t))M + (1 - \omega^2_{s,i,p}(t))M,\ t = 0, \ldots T-1; \forall i \in \Omega; \forall p \in P_i; \forall s \in S \tag{35}$$

$$q^d_{s,i,p}(t) \geq q^u_{i,p} - (1 - \omega^1_{s,i,p}(t))M - \omega^2_{s,i,p}(t)M,\ t = 0, \ldots T-1; \forall i \in \Omega; \forall p \in P_i; \forall s \in S \tag{36}$$

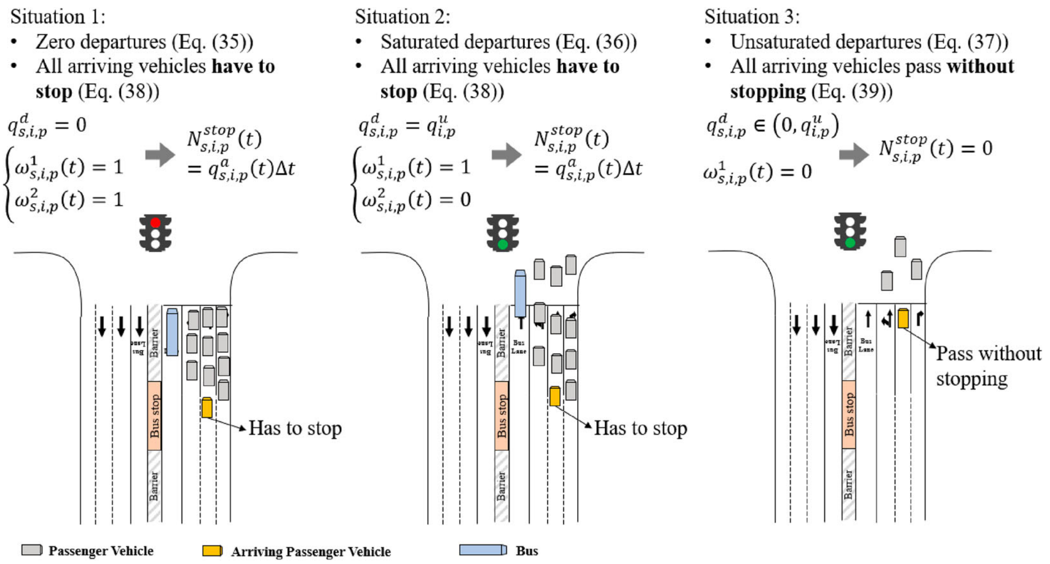


**Figure 5.** Situations of passenger vehicle departures.

$$-\omega^1_{s,i,p}(t)M + 0 + \epsilon \le q^d_{s,i,p}(t) \le q^u_{i,p} - \epsilon + \omega^1_{s,i,p}(t)M,\ t = 0, \ldots T-1; \forall i \in \Omega; \forall p \in P_i; \forall s \in S \tag{37}$$

$$-(1-\omega^1_{s,i,p}(t))M + q^a_{s,i,p}(t)\Delta t \le N^{stop}_{s,i,p}(t) \le q^a_{s,i,p}(t)\Delta t + (1-\omega^1_{s,i,p}(t))M,\ t = 0, \ldots T-1; \forall i \in \Omega; \forall p \in P_i; \forall s \in S \tag{38}$$

$$-\omega^1_{s,i,p}(t)M \le N^{stop}_{s,i,p}(t) \le \omega^1_{s,i,p}(t)M,\ t = 0, \ldots T-1; \forall i \in \Omega; \forall p \in P_i; \forall s \in S \tag{39}$$

where $q^u_{i,p}$ denotes the saturated passenger vehicle departures of phase $p$ at intersection $i$; $\omega^2_{s,i,p}(t)$ is an auxiliary binary variable for modelling.

The passenger vehicles at an intersection are identified based on the departure profile of the upstream intersection. Three types of upstream vehicles contribute to the downstream arriving vehicles: vehicles passing through, left-turn vehicles, and right-turn vehicles, as shown in Figure 6. We consider the outbound-direction phase as an example. In the arterial approach phase, the number

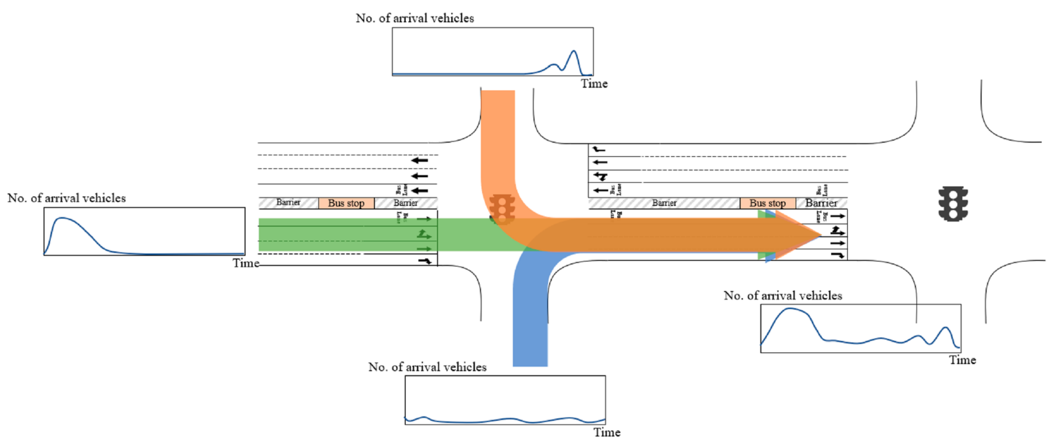


**Figure 6.** Composition of vehicles from upstream intersection.

of passenger vehicles arriving at intersection $i$ at time step $t$ depends on the departure of passenger vehicles at the upstream intersection at time step $t - t^a_{i-1} - O_i + O_{i-1}$ (Eq. (40)). The volumes of the arterial input approaches at the first intersection of the artery and side streets are known (Eq. (41)–(42)).

$$q^a_{s,i,p}(t) = \theta_{i,p}(q^d_{s,i-1,p^t_{i-1}}(\hat{t}) + q^d_{s,i-1,p^l_{i-1}}(\hat{t}) + \tilde{q}^a_{i-1,m^R_{i-1}}(\hat{t})),\ \hat{t} = t - t^a_{i-1} - O_i + O_{i-1},$$
$$t = 0, \dots T-1; \forall i \in \Omega, i \neq 1; p = p^a_i; \forall s \in S \tag{40}$$

$$q^a_{s,i,p}(t) = \sum_{m=1}^{12} \gamma_{i,p,m}\tilde{q}^a_{i,m}(t), t = 0, \dots T-1; \forall i \in \Omega; \forall p \in P^d_i; \forall s \in S \tag{41}$$

$$q^a_{s,1,p}(t) = \sum_{m=1}^{12} \gamma_{1,p,m}\tilde{q}^a_{1,m}(t), t = 0, \dots T-1; p = p^a_i; \forall s \in S \tag{42}$$

where $\theta_{i,p}$ denotes the turning ratio of phase $p$ at intersection $i$; $\tilde{q}^a_{i-1,m^R_{i-1}}(t)$ denotes the number of input arrival passenger vehicles of movement $m^R_{i-1}$ at intersection $i-1$; $m^R_{i-1}$ denotes the right turn movement that goes from the side street to the artery at intersection $i-1$; $p^t_{i-1}$ and $p^l_{i-1}$ denote the phase indices of the movements that go through on the artery approach and turn left from the side street to the artery, respectively; $P^c_i$ and $P^d_i$ denote sets of phases from the artery approaches and the side street approaches, respectively; $P^u_i$ denotes the phase set of ring 1; $\gamma_{i,p,m}$ is a binary parameter related to the phase-movement corresponding relation at intersection $i$. It is one, if phase $p$ corresponds to movement $m$; otherwise, it is zero.

The vehicle departure profile at time step $t$ depends on the phase states. If vehicles from phase $p$ are discharged at time step $t$, the number of departure passenger vehicles $q^d_{s,i,p}(t)$ can be either a saturated departure with a queue present or an unsaturated departure which equals the number of arriving passenger vehicles when there is no queue, i.e. $q^d_{s,i,p}(t)$ should be the smaller value between the saturated vehicle departures and queue length. Otherwise, $q^d_{s,i,p}(t)$ is zero, as shown in Eqs. (43)–(44). The boundary condition at the start of the control horizon is expressed by Eqs. (45)–(46). $p^a_i$ denotes the prioritised phase index of the outbound direction at intersection $i$.

$$q^d_{s,i,p}(t) = \begin{cases} \min\{q^u_{i,p}, l_{s,i,p}(t-1) + q^a_{s,i,p}(t)\},\ if\ t \in [\tilde{G}^r_{i,p}, \tilde{G}^e_{i,p}) \cup [G^r_{s,i}, G^e_{s,i}) \\ 0, otherwise \end{cases},$$
$$t = 1, \dots T-1; p = p^a_i; \forall i \in \Omega; \forall s \in S \tag{43}$$

$$q^d_{s,i,p}(t) = \begin{cases} \min\{q^u_{i,p}, l_{s,i,p}(t-1) + q^a_{s,i,p}(t)\},\ if\ t \in [\tilde{G}^r_{i,p}, \tilde{G}^e_{i,p}) \\ 0, otherwise \end{cases},$$
$$t = 1, \dots T-1; p \in P^u, p \neq p^a_i; \forall i \in \Omega; \forall s \in S \tag{44}$$

$$q^d_{s,i,p}(0) = \begin{cases} \min\{q^u_{i,p}, l^0_{s,i,p} + q^a_{s,i,p}(0)\},\ if\ t \in [\tilde{G}^r_{i,p}, \tilde{G}^e_{i,p}) \cup [G^r_{s,i}, G^e_{s,i}) \\ 0, otherwise \end{cases},$$
$$\forall i \in \Omega; p \in P^u_i, p = p^a_i; \forall s \in S \tag{45}$$

$$q^d_{s,i,p}(0) = \begin{cases} \min\{q^u_{i,p}, l^0_{s,i,p} + q^a_{s,i,p}(0)\},\ if\ t \in [\tilde{G}^r_{i,p}, \tilde{G}^e_{i,p}) \\ 0, otherwise \end{cases},$$
$$\forall i \in \Omega; p \in P^u_i, p \neq p^a_i; \forall s \in S \tag{46}$$

The total passenger vehicle delay $\mathbb{D}^a_s$, is given by the summation of the vehicle delays of all phases at all intersections, as shown in Eq. (47).

$$\mathbb{D}^a_s = \sum_i \sum_p D^a_{s,i,p}, \forall s \in S \tag{47}$$

### 3.2. Objective functions

Owing to the SAA method used to model the stochastic optimisation, the optimal signal coordination variables, which are the uniform cycle length and offsets, are determined by solving the following offline problem:

(P1)

$$\min J_1 = \frac{1}{|S|}\sum_{s\in S}(K^{a,f}N^{p,a}\mathbb{D}_s^a + K^{b,f}N^{p,b}\mathbb{D}_s^b) \tag{48}$$

s.t. Eqs. (1)–(47).

The coefficients $K^{a,f}$ and $K^{b,f}$ are determined by policymakers to balance the delay values between passenger vehicles and buses. $N^{p,a}$ and $N^{p,b}$ denote the average numbers of passengers in passenger vehicles and on buses, respectively. Therefore, the objective of P1 is to minimise the total weighted passenger delays of passenger vehicles and buses. This is used as the performance measure because it is tangible, commonly used, and calculable. The numbers of continuous variables, integer variables, and constraints are $O(T \times S \times I \times P)$ in P1.

P1 obtains an optimal signal coordination plan considering the uncertainties in bus operations, which also affects passenger vehicle delays, by giving signal priority. In real-world bus operations, the fixed cycle length and offsets obtained by P1 are applied. For a specific bus arrival and running information in a cycle in real-time operation, online signal priority optimisation P2 is conducted to realise bus signal priority control. The online signal priority control (including the priority green period start and end points at each intersection) and bus trajectories along the artery (including bus arrival/departure times at each stop and intersection) are determined by solving the following problem:

(P2)

$$\min J_2 = K^{a,n}N^{p,a}\mathbb{D}_s^a + K^{b,n}N^{p,b}\mathbb{D}_s^b \tag{49}$$

Constraints include Eqs. (3)–(47), for the sample set that only contains one realised scenario because the bus arrivals are known, and the bus dwell time and travel time have been predicted as parameters for the sample. The coefficients $K^{a,n}$ and $K^{b,n}$ are also decided by policymakers. The numbers of continuous variables, integer variables, and constraints are $O(T \times S \times I \times P)$ in P2.

P1 and P2 are applied in different stages. P1 is designed to optimise the cycle length and offsets offline using historical data over a period. The optimal solutions to P1 include a set of bus trajectory samples with signal priority strategies. Only the optimal cycle length and offsets are applied to real-world operations for intersection control. P2 is designed to optimise the real-time signal priority and bus arrival/departure time at stops and intersections with real-time bus operational information. P2 is a specific scenario of P1 with a set of deterministic parameters. Real-time signal priority strategies calculated by P2 are dynamically applied. Therefore, P2 can be considered a subroutine of P1. P1 and P2 cannot be merged to one because they have different requirements for update frequency. Signal coordination plans optimised by P1 are more suitable to be adjusted over a longer period during which vehicles pass through multiple intersection, whereas signal priority and bus trajectories are more suitable to be optimised in real time to adapt to varying bus operating states. We separate P2 from P1 to clarify the application of offline signal coordination and online signal priority processes.

## 4. Solution algorithm

The biggest challenge in solving the proposed SP (P1) lies in its large dimensions, and the decision variable cycle length $C$ is divided in Eqs. (23)–(24). The number of samples increased linearly with the size of P1. Thus, a scenario-based heuristic algorithm (SBHA) is designed to separate the calculation of the signal coordination plan from the computation of the signal priority control and bus trajectories, which differ for different samples. In the SBHA, the cycle length is determined by enumeration, and the offsets are determined based on the genetic algorithm (GA):

Step 0: Initialise cycle length $C = C_0$ and the offset population in GA.

Step 1: Initialise iteration $\kappa = 1$.

Step 2: Select 50% of the individuals in the population based on their performance.

Step 3: Arithmetic crossover, non-uniform mutation, and merging the selected and mutated populations as offspring.

Step 4: Calculate fitness $F_{\kappa,ind}$ for every individual by $F_{\kappa,ind} = \frac{1}{|S|}\sum_{s\in S} F_{\kappa,ind,s}$. $F_{\kappa,ind,s}$ is the fitness of individual *ind* in scenario *s* by solving P2.

Step 5: Select the best individual $O_\kappa^*$ with the best fitness $F_\kappa^*$.

Step 6: If $\kappa > 1$ and $|F_\kappa^* - F_{\kappa-1}^*| \leq \varepsilon$, go to Step 7. Otherwise, $\kappa = \kappa + 1$ and go to Step 2.

Step 7: If $C + \Delta C \leq \hat{C}$, $F_C = F_\kappa^*$, update $C = C + \Delta C$, and go to Step 1. Otherwise, select the best individual $F_C^*$ in $F_C$.

Specifically, in Step 4, P2 is solved independently in every scenario using parallel computation. The large dimension of P2 lies in the combination of feasible signal priority plans. Thus, P2 is solved by selecting the signal priority plan with the least system delay from the signal plans, calculated by considering the arrival times of the buses at every intersection. Notably, the cycle length and offsets are computed offline based on P1 in advance by the proposed SBHA, whereas the dynamic signal priority strategies are calculated online based on P2 in Steps 4.0 to 4.5:

Step 4.0: Initialise bus index $y = 1$.

Step 4.1: Calculate the arrival time at the downstream intersection $t_{s,y}^{bus}$ of bus *y* and signal priority plan $TSP_y$.

Step 4.2: If $y + 1 \leq Y$, $y = y + 1$ and go to Step 4.1.

Step 4.3: Merge the signal priority plans $TSP_{y_1}$ and $TSP_{y_2}$ for every pair of signal priority plans into $TSP_z^m$ if they do not conflict. Otherwise, $TSP_{z_1}^m = TSP_{y_1}$ and $TSP_{z_2}^m = TSP_{y_2}$.

Step 4.4: Calculate system delay $D_z$ of every $TSP_z^m$.

Step 4.5: Select the best $TSP_z^*$ with the least system delay $D_z^*$.

*Remark*: Owing to CV technologies, buses can adjust their speeds or trajectories to avoid stops at intersections, e.g. slow down (Varga et al. 2020), to reduce deceleration/acceleration delay at intersections.

## 5. Case study

In this section, we evaluate the benefits of the proposed stochastic priority-integrated coordination (SPIC) for arterial signal control in terms of efficiency and coordination. The total delay represents the efficiency, and the stop times indicate the coordination along the artery. To validate the effectiveness of SPIC, we compare it with four other methods. The original plan (ORGP) serves as the benchmark strategy. We also test stochastic priority-integrated signal coordination-passenger vehicle (SPIC-PV) only, which does not include signal priority but considers passenger vehicles alone to evaluate the effects of signal priority. We also compare MAXBAND and PMBAND to analyse the performance differences between the band-oriented models and delay minimisation models.

### 5.1. Simulation setup

A typical three-intersection artery in Zhengzhou, China is used. Figure 7 shows the artery layout, signal control plans, passenger vehicle travel time, and intersection delays. The orange line represents the

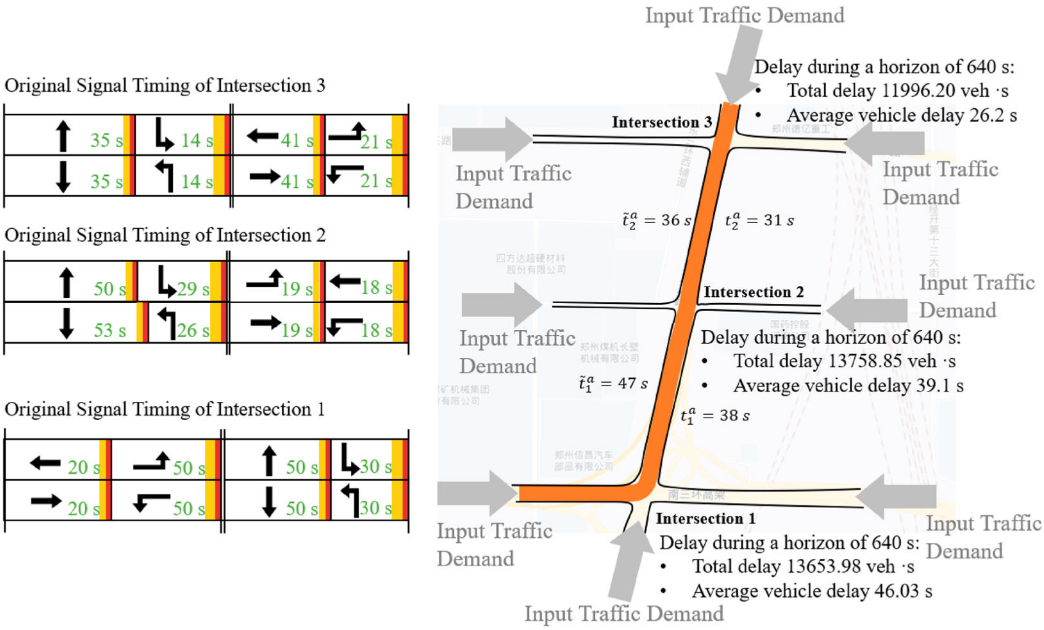


**Figure 7.** Layout and information of applied artery.

**Table 2.** Passenger vehicle and bus information inputs.

| Passenger Vehicle Input Data | | | | | | | | |
|---|---|---|---|---|---|---|---|---|
| Saturated Flow (pcu/h) | Phase 1 | Phase 2 | Phase 3 | Phase 4 | Phase 5 | Phase 6 | Phase 7 | Phase 8 |
| I 1 | 3300 | 1550 | 3300 | 1550 | 4950 | 1550 | 3300 | 1550 |
| I 2 | 3300 | 1550 | 1163 | 1650 | 3300 | 1550 | 868 | 3100 |
| I 3 | 3300 | 1450 | 4950 | 1550 | 3300 | 1550 | 1650 | 1550 |

| Volume (pcu/h) or Turning Ratio | West-bound | | | South-bound | | | East-bound | | | North-bound | | |
|---|---|---|---|---|---|---|---|---|---|---|---|---|
| Turning | L | T | R | L | T | R | L | T | R | L | T | R |
| I 1 | 152 | 32 | 4 | 84 | 316 | 16 | 56 | 52 | 4 | 30% | 65% | 5% |
| I 2 | 48 | 24 | 24 | 15% | 80% | 5% | 48 | 60 | 12 | 20% | 75% | 5% |
| I 3 | 96 | 144 | 24 | 30% | 60% | 10% | 252 | 348 | 36 | 48 | 372 | 204 |

| Bus Input Data | Outbound | | | Inbound | | |
|---|---|---|---|---|---|---|
| Travel time (second) | Origin to I 1 | I 1 to I 2 | I 2 to I 3 | I 3 to I 2 | I 2 to I 1 | I 3 to Origin |
| (Mean, standard deviation) | (12.5, 3.4) | (54.24, 8.34) | (48.23, 17.1) | (53.9, 5.8) | (58.65, 4.63) | (18.3, 5.6) |

| | Outbound buses | | Inbound buses | |
|---|---|---|---|---|
| Dwell time (second) | I 1 to I 2 | I 2 to I 3 | I 3 to I 2 | I 2 to I 1 |
| (Mean, standard deviation) | (20, 2) | (20, 2) | (20, 2) | (20, 2) |

Note: I * denotes Intersection *; L, T, and R denote left turn, through going, and right turn, respectively; the percentages are the turning ratios.

arterial route. Each intersection has four arms. Phases 1, 3, 5, and 7 have yellow and all-red times of 3 s, whereas phases 2, 4, 6, and 8 have 6 s. The original green splits remain the same as those in the real world. Table 2 presents the saturated flow rates, passenger vehicle volumes, and turning ratios.

The artery has a low traffic demand and delays, as shown in Figure 7. We conduct a sensitivity analysis of the traffic demand to evaluate its effects. The cycle lengths range from 80 to 160 s at 10-second intervals. In GA, the population size is 40. The crossing probability is 90%, whereas the variation probability is 20%. The variation parameter is 3. The sufficiently small number $\epsilon$ is 0.001. Ten scenarios are considered in the experiments; the scenarios remain the same during the GA tests to save time and computation resources. The maximum number of iterations is 120, and the algorithm converges if the best individual remains unchanged for 40 iterations. The coefficients $K^{a,f}$ and $K^{a,n}$ are both 0.25, whereas $K^{b,f}$ and $K^{b,n}$ are both 0.75. The time step $\Delta t$ is 1 s. The optimisation horizon is 640 s.

For the bus information, the bus segment travel time and dwell time follow Gaussian distributions with the parameters listed in Table 2. Only positive values from the Gaussian distributions are used; negative values are discarded and regenerated. The bus arterial arrival time follows a uniform distribution within the optimisation horizon. The average bus arrival headway at the artery is 60 s in each direction. The maximum green extension and advance time are both 12 s.

These methods are implemented using Python 3.7.0. The experiments are conducted on a desktop computer with an Intel CPU 1.60 GHz and 8.00 GB memory. A parallel computation with two threads is utilised. The average computation times for P1 and P2 are $3.35 \times 10^5$ s and 0.24 s, respectively. The computation time can be further reduced with more computers, which is feasible despite the relatively long computation time of P1 because the cycle length and offsets are determined offline. The solution time for P2 is sufficiently short to derive the real-time signal priority to accommodate time-varying bus operations.

### 5.2. Results and discussions

The total delays for the passenger vehicles and buses are measured, with the cycle lengths and offsets optimised using P1 and other comparison methods. Table 3 presents the results of the signal coordination plan. Subsequently, P2 is conducted with the background signal coordination control of ORGP, MAXBAND, PMBAND, P1 of SPIC-PV, and P1 of SPIC. The same bus priority strategies are used for the five background signal coordination plans listed in Table 3. We test 50 stochastic bus operation scenarios and calculate the average delays under five background signal coordination plans. Figure 8 shows the results, with the proposed SPIC achieving the best performance compared to ORGP, MAXBAND, PMBAND, and SPIC-PV. The total and bus delays are reduced by 36% and 56%, respectively, compared to ORGP. It indicates the cooperation between the online signal priority and offline SP performs well owing to the considerations of the stochastic signal priority. SPIC also has a 23% delay reduction compared to MAXBAND and a 46% reduction compared to PMBAND. PMBAND increases delays for passenger vehicles and buses due to its lack of consideration of the stochastic signal priority. Comparisons among the SPIC, MAXBAND, and PMBAND show that delays represent traffic conditions better than progression bandwidths. Therefore, the proposed SPIC effectively reduces system delays under time-varying bus operations.

In addition to travel delays, intersection stop times reflect the smoothness of travel along the artery and signal coordination effects. Table 4 lists the average stop times and their decreases compared to the ORGP at intersections. SPIC can significantly reduce the stop times of passenger vehicles at intersections from 2.07 times to 1.42 times, a 31.4% reduction. However, MAXBAND has the lowest stop time, followed by PMBAND, because it creates bands where vehicles can pass without stopping.

**Table 3.** Optimal solutions.

| | | Offsets (second) | | |
|---|---|---|---|---|
| Methods | Cycle length | Intersection 1 | Intersection 2 | Intersection 3 |
| ORGP | 120 | 0 | 0 | 0 |
| MAXBAND | 80 | 0 | 33 | 70 |
| PMBAND | 160 | 0 | 123 | 72 |
| SPIC-PV | 80 | 0 | 2 | 9 |
| SPIC | 80 | 0 | 2 | 5 |

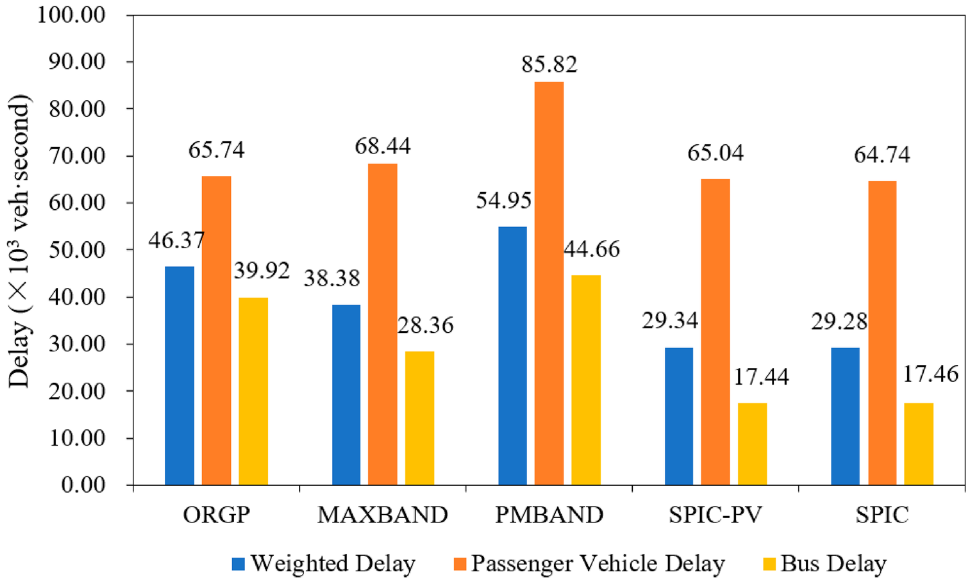


**Figure 8.** Delays in online cases.

**Table 4.** Passenger vehicle and bus stop times at intersections.

| | Passenger Vehicles | | Buses | |
|---|---|---|---|---|
| Methods | Average Stop Times | Decrease of Average Stop Times (%) | Average Stop Times | Decrease of Average Stop Times (%) |
| ORGP | 2.07 | – | 1.46 | – |
| SPIC | 1.42 | 31.40 | 1.31 | 10.27 |
| SPIC_PV | 1.40 | 32.37 | 1.44 | 1.37 |
| MAXBAND | 1.23 | 40.58 | 1.43 | 2.05 |
| PMBAND | 1.32 | 36.23 | 1.33 | 8.90 |

PMBAND also establishes bus bands that slightly impact passenger vehicle bands. For buses, the stop-time reductions are limited. SPIC decreases the bus stop times by 10.27%, followed by the PMBAND (8.9%). SPIC-PV and MAXBAND do not consider the bus benefits and thus show little improvement in the bus efficiency. These observations align with our intuition and the SPIC can reduce both vehicle delays and stop times at intersections.

### *5.3. Sensitivity analyses*

Sensitivity analyses are conducted to evaluate the effects of the input parameters on the method performance. The bus travel time and dwell time deviation are stochastic, affecting the bus arrival times at each intersection, further influencing the online signal priority. The traffic demands of the passenger vehicles on the artery also affect the queue lengths and delays. The weights of the passenger vehicles and buses in the objective function directly influence the benefit balance between the two modes. A deterministic method is compared with the SPIC to evaluate the contribution of the stochasticity considerations of the bus operations. ORGP is used as the benchmark and considered a starting point for improvements in the delay-reduction calculations. The cycle lengths for SPIC and ORGP are 80 and 120 s, respectively.

### 5.3.1. Deviation of bus travel time and dwell time

Six levels of the standard deviation (SD) for the bus dwell time and travel time are tested, ranging from 0 to 25 s. Figure 9 shows the decrease in the total delay, passenger vehicle delay, and bus delay with varying SD for bus dwell times. The total delay improvement decreases slightly from $\sim 50\%$ to $\sim 42\%$ as the SD increases. A higher level of bus operation uncertainty causes the deterministic solution to deviate from the optimal solution. The reduction in bus delays mainly contributes to the total delay decrease, ranging from 59.89% to 69.04%. Thus, the proposed SPIC method handles the bus dwell-time uncertainty well. The bus delay always decreases with the SPIC, whereas the passenger vehicle delay increases slightly, attributed to the benefit shifting from passenger vehicles to buses; however, the impacts on passenger vehicles are limited, ranging from −6.88% to −10.98%. Similar trends are observed in Figure 10 with varying SD for bus travel times because they both affect the bus arrival times at the downstream intersections simultaneously. Overall, the SPIC performs well with fluctuations in the bus dwell and travel times.

### 5.3.2. Traffic demands

Ten levels of traffic demands have been tested to evaluate the performance of the method under different passenger vehicle demands. The traffic demand is the product of the demand factor and the traffic demand in the base case. The demand factor varies from 0.5–5. Figure 11 shows the delay decrease in SPIC compared to ORGP at different traffic demands. For traffic demand factor $\leq 2.5$, the total delay improvements decrease from 60.47% to 28.93%. For a traffic demand factor $> 2.5$, the method performance increases slightly from $\sim 31\%$ to $\sim 41\%$ and drops back to 35.43% for a traffic demand factor of 5. The bus delay reduction remains steady at 65% to 73% because the bus arrivals are not affected by the varying passenger vehicle demands. The passenger vehicle delay reduction increases from negative to positive percentages with increasing traffic demand, except for demand factors of 0.5 and 5, thus suggesting that SPIC improves passenger vehicle efficiency at high demands (demand factors $\geq 2$). When the traffic demand factor is 0.5, there is little traffic on the road, and signal coordination results in only a marginal improvement ($\sim 7\%$). Passenger vehicle delay reduction stays at $\sim 30\%$ for demand factors $\geq 4$. At a traffic demand factor of 5, the traffic demand approaches capacity, resulting in a slight drop in delay improvements. In summary, the SPIC performs well with

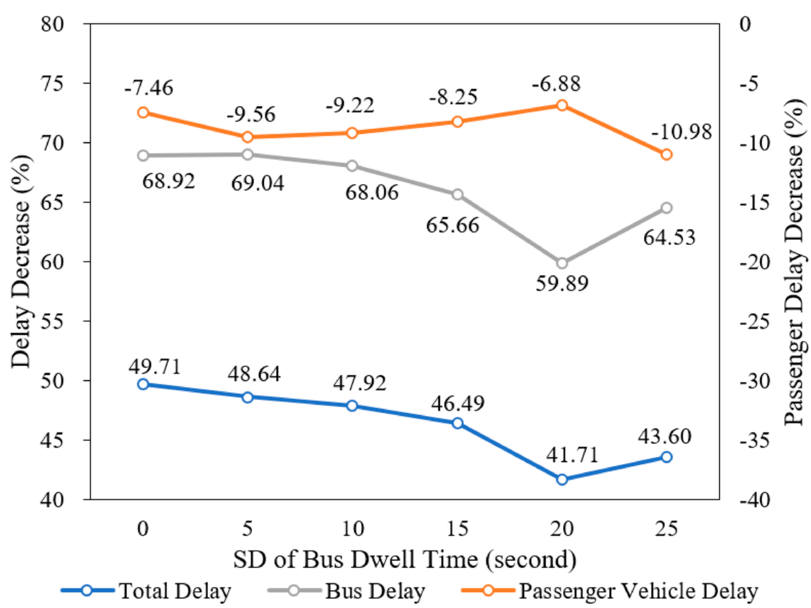


**Figure 9.** Impacts of SD of bus dwell time.

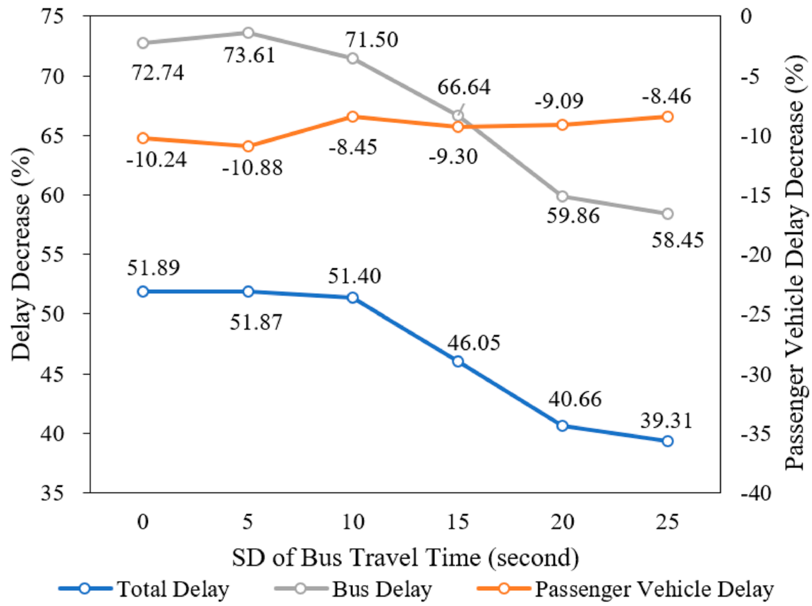


**Figure 10.** Impacts of SD of bus travel time.

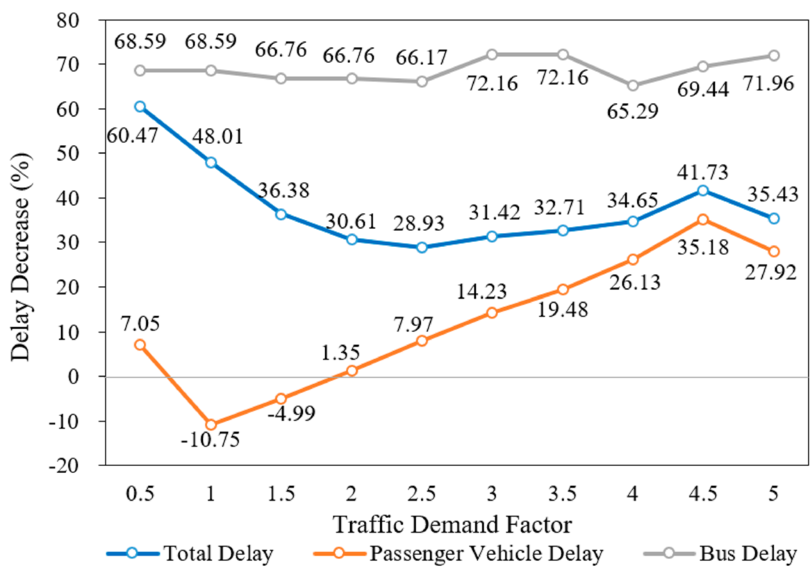


**Figure 11.** Impacts of traffic demands on delay.

varying passenger vehicle traffic demands, bringing more efficiency benefits to passenger vehicles at higher demands. The bus delays are not sensitive to the varying passenger vehicle demands.

### 5.3.3. *Weights in the objective function*

The effects of the weights $K^{a,f}$ and $K^{b,f}$ on the objective function of P1 are tested by varying $K^{b,f}$ from zero to one. Both weights are standardised between zero and one. Figure 12 shows the delay decrease percentage of SPIC compared to ORGP with varying $K^{b,f}$. As $K^{b,f}$ increases, the overall performance steadily improves. Specifically, the passenger vehicle delay reduction slightly decreases from $\sim -4\%$

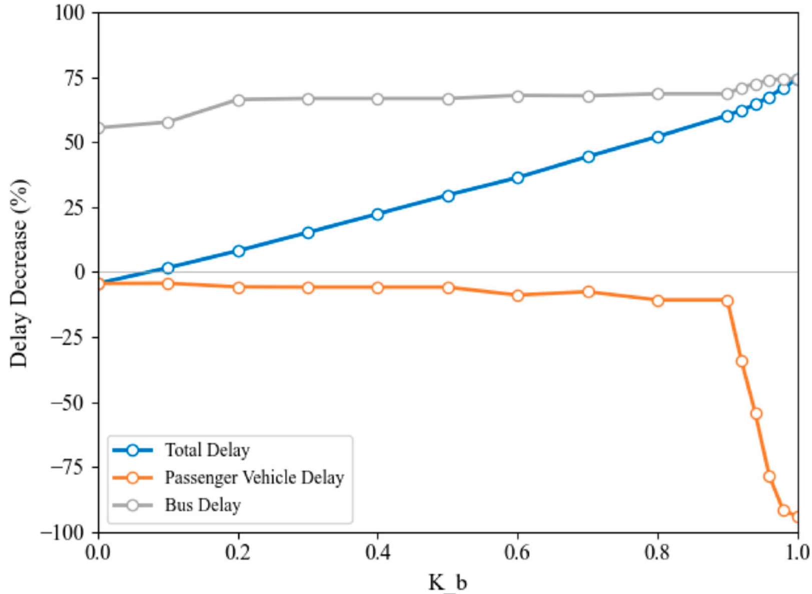


**Figure 12.** Impacts of weights in the objective function on delay.

to $\sim -10\%$ for $K^{b,f} \leq 0.9$ and drops drastically for $K^{b,f} > 0.9$. Additional experiments with $K^{b,f}$ values of 0.92, 0.94, 0.96, and 0.98 confirm this trend. When $K^{b,f}$ approaches one, passenger vehicle benefits are almost not included in the objective function, leading to a significant reduction in passenger vehicle delay improvements. When $K^{b,f} = 0$, the bus delay is reduced by approximately 55%, primarily because of the adjustment in the cycle length. These observations provide reference values for setting $K^{b,f}$ and $K^{b,f}$, including a) highlight bus benefits for $0.2 \leq K^{b,f} \leq 0.9$; b) SPIC performance is not sensitive for $0.2 \leq K^{b,f} \leq 0.9$; and c) avoid setting $K^{b,f}$ in the range of (0.9, 1] because it significantly increases the passenger vehicle delay.

### *5.3.4. Uncertainty considerations*

Experiments using deterministic methods are designed to evaluate the effects of the scenario-based method compared with the deterministic method. In the deterministic method, only one scenario is conducted to calculate the optimal signal coordination plan, i.e. the cycle length and offsets. In this scenario, the bus travel time and dwell time are set as the mean values of the distributions used in the stochastic method, with the bus arterial arrival times sampled according to the same uniform distribution used in the stochastic method. The average performance of the scenarios conducted with P2 is compared between the optimal signal coordination plans from the stochastic and deterministic methods. Figure 13 shows the delay performances of the ORGP, SPIC, and deterministic methods. The SPIC outperforms the deterministic method, with a delay reduction of $\sim 36\%$ and a bus delay reduction of $\sim 56\%$. The deterministic method achieves $\sim 24\%$ overall delay reduction and $\sim 39\%$ bus delay reduction, implying that not considering the bus operation uncertainty in the deterministic method leads to suboptimality in the coordinated signal control. Histograms of the delays of the ten deterministic experiments are shown in Figure 14 to illustrate their performance distribution. The total weighted delay varies from $\sim 28000$ s to $\sim 40000$ s, which is a large deviation. Passenger vehicle delays range from $\sim 66000$ s to $\sim 69500$ s, whereas bus delays span a wide range from $\sim 15000$ s to $\sim 32500$ s – a reasonable result because stochasticity is related to bus operations. Compared to the histograms of the stochastic method, the delay distributions in the deterministic experiments tend to have higher values and larger ranges. Therefore, the SPIC effectively handles bus operation stochasticity in the signal coordination control.

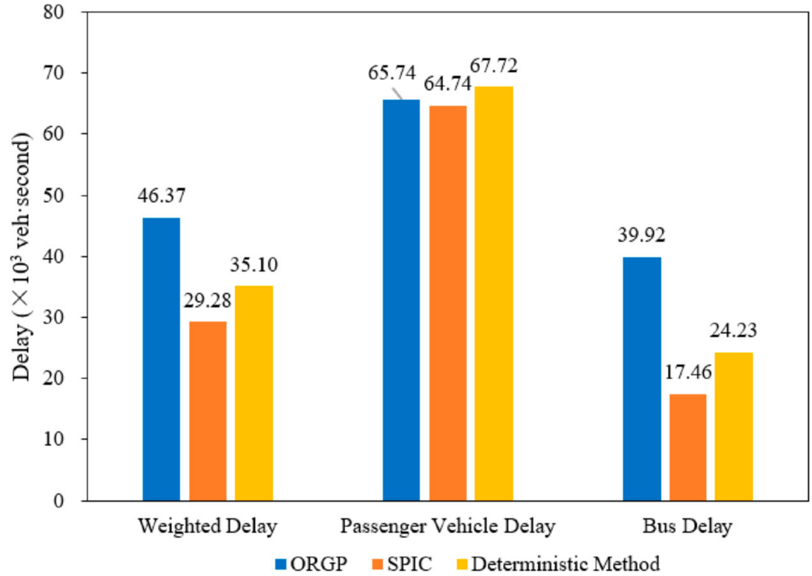


**Figure 13.** Delay comparisons between deterministic and stochastic methods.

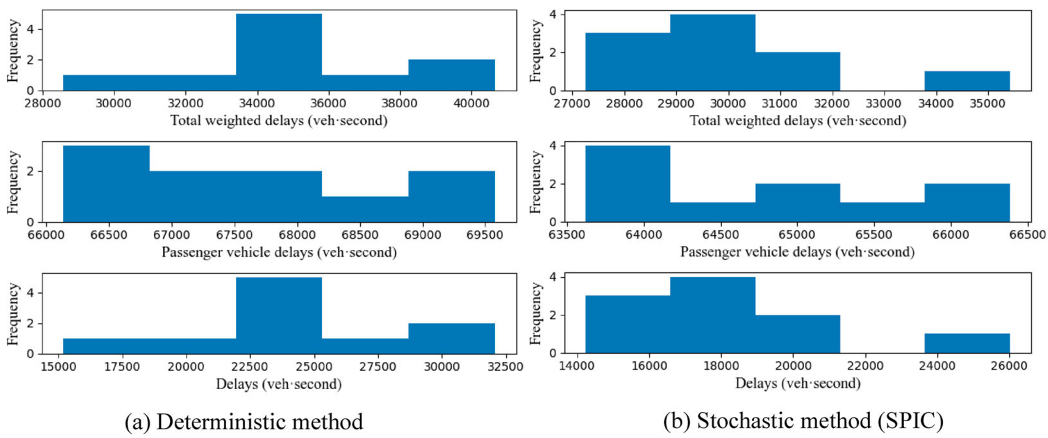


**Figure 14.** Histograms of delays with deterministic and stochastic methods. (a) Deterministic method; (b) Stochastic method (SPIC).

## 6. Conclusions

This study proposes a stochastic priority-integrated signal coordination (SPIC) method that combines an SP approach to determine the uniform cycle length and offsets along an artery and an MINLP for determining signal priority strategies. In the SPIC, the bus travel time, dwell time, and arterial arrival time are stochastic in a CV environment, where buses share real-time information and receive speed advisories. The objective is to minimise the weighted total passenger delays for passenger vehicles and buses. This novel method estimates passenger vehicle delays by considering the signal coordination control and stochastic signal priority. SPIC determines the cycle length and offsets by solving the SP offline, and signal priority strategies are determined online using MINLP to adapt to real-time bus operating conditions. Numerical studies validate the advantages of the proposed methods, reducing the total delay and bus delay by up to 36% and 56%, respectively. SPIC also enhances the system efficiency and arterial coordination effects by reducing the vehicle stop times. Sensitivity analyses show that: a) SPIC performs well with varying bus travel time, dwell time, and traffic demands for vehicles, b) it brings more efficiency to vehicles with higher traffic demands and benefits buses within a range of $0.2 \leq K^{b,f} \leq 0.9$, while avoiding $K^{b,f} \in (0.9, 1]$ which significantly increases vehicle delays, and c) SPIC effectively handles bus operational stochasticity compared to deterministic methods.

While this study focuses on arterial traffic, the extension of the proposed method to a network-level area with multiple arteries is another interesting research topic. Automatic bus trajectory planning is assumed with a given arrival time at an intersection or stop. Future studies could also include trajectory planning for buses and passenger vehicles while considering energy consumption and vehicle emissions.

## Disclosure statement

No potential conflict of interest was reported by the author(s).


## Funding

This work was supported by the National Natural Science Foundation of China under Grant Nos. 52131204 and 72101186, Fundamental Research Funds for the Central Universities No. 2022-5-YB-05, No.16002150143, and the China Scholarship Council. The authors declare no conflicts of interest.



## ORCID

*Wanjing Ma* http://orcid.org/0000-0002-9403-3174


## References


Beak, Byungho, K. Larry Head, and Yiheng Feng. 2017. “Adaptive Coordination Based on Connected Vehicle Technology.” *Transportation Research Record: Journal of the Transportation Research Board* 2619 (1): 1–12. https://doi.org/10.3141/2619-01

Bian, Bomin, Ning Zhu, Shuai Ling, and Shoufeng Ma. 2015. “Bus Service Time Estimation Model for a Curbside Bus Stop.” *Transportation Research Part C: Emerging Technologies* 57 (August): 103–121. https://doi.org/10.1016/j.trc.2015.06.011

Chen, Yen-Hsiang, Yao Cheng, and Gang-Len Chang. 2021. “Incorporating Bus Delay Minimization in Design of Signal Progression for Arterials Accommodating Heavy Mixed-Traffic Flows.” *Journal of Intelligent Transportation Systems* 27 (2): 1–30.

Cho, H.-J., T.-J. Huang, and C.-C. L. Huang. 2019. “Path-Based MAXBAND with Green-Split Variables and Traffic Dispersion.” *Transportmetrica B: Transport Dynamics* 7 (1): 726–740. https://doi.org/10.1080/21680566.2018.1493624

Chow, Andy H. F., Z. C. Su, E. M. Liang, and R. X. Zhong. 2021. “Adaptive Signal Control for Bus Service Reliability with Connected Vehicle Technology via Reinforcement Learning.” *Transportation Research Part C: Emerging Technologies* 129 (August): 103264. https://doi.org/10.1016/j.trc.2021.103264

Das, Debashis, Niraj Vasant Altekar, and K. Larry Head. 2023. “Priority-Based Traffic Signal Coordination System with Multi-Modal Priority and Vehicle Actuation in a Connected Vehicle Environment.” *Transportation Research Record: Journal of the Transportation Research Board* 2677 (5): 666–681. https://doi.org/10.1177/03611981221134627

Estrada, Miquel, Josep Mensión, Josep M. Aymamí, and Laura Torres. 2016. “Bus Control Strategies in Corridors with Signalized Intersections.” *Transportation Research Part C: Emerging Technologies* 71 (October): 500–520. https://doi.org/10.1016/j.trc.2016.08.013

Florek, Krzysztof. 2020. “Arterial Traffic Signal Coordination for General and Public Transport Vehicles Using Dedicated Lanes.” *Journal of Transportation Engineering, Part A: Systems* 146 (7): 04020051. https://doi.org/10.1061/JTEPBS.0000374

Gartner, Nathan, Susan Assmann, Fernando Lasaga, and Dennis Hou. 1990. “MULTIBAND – A Variable-Bandwidth Arterial Progression Scheme.” *Transportation Research Record Journal of the Transportation Research Board* 1287 (January): 212–222.

He, Qing, K. Larry Head, and Jun Ding. 2014. “Multi-Modal Traffic Signal Control with Priority, Signal Actuation and Coordination.” *Transportation Research Part C: Emerging Technologies* 46 (September): 65–82.

Hu, Jia, Zihan Zhang, Yongwei Feng, Zhongxiao Sun, Xin Li, and Xianfeng Yang. 2021. “Transit Signal Priority Enabling Connected and Automated Buses to Cut Through Traffic.” *IEEE Transactions on Intelligent Transportation Systems* 23 (7): 8782–8792.

Johar, Amita, S. S. Jain, and P. K. Garg. 2016. “Prediction of Bus Travel Time Using ANN: A Case Study in Delhi.” Transportation Research Procedia, International Conference on Transportation Planning and Implementation Methodologies for Developing Countries (12th TPMDC) Selected Proceedings, IIT Bombay, Mumbai, India, 10-12 December 2014, 17 (January): 263–272.

Li, Lubing, Wei Huang, Andy H. F. Chow, and Hong K. Lo. 2022. "Two-Stage Stochastic Program for Dynamic Coordinated Traffic Control Under Demand Uncertainty." *IEEE Transactions on Intelligent Transportation Systems* 23 (8): 12966–12976. https://doi.org/10.1109/TITS.2021.3118843

Li, Lubing, Wei Huang, and Hong K. Lo. 2018. "Adaptive Coordinated Traffic Control for Stochastic Demand." *Transportation Research Part C: Emerging Technologies* 88 (March): 31–51.

Li, Jiali, Yugang Liu, Nan Zheng, Liying Tang, and Hongbo Yi. 2021. "Regional Coordinated Bus Priority Signal Control Considering Pedestrian and Vehicle Delays at Urban Intersections." *IEEE Transactions on Intelligent Transportation Systems* 23 (9): 16690–16700.

Liang, Shidong, Rongmeng Leng, Hu Zhang, and Jing Zhao. 2023. "Two-Stage Transit Signal Priority Control Method to Improve Reliability of Bus Operation Considering Stochastic Process." *Transportation Research Record: Journal of the Transportation Research Board* 2677 (2): 1713–1727. https://doi.org/10.1177/03611981221113318

Liang, Zijun, Yun Xiao, and Yun-Pang Flötteröd. 2021. "An Overlapping Phase Approach to Optimize Bus Signal Priority Control under Two-Way Signal Coordination on Urban Arterials." *Journal of Advanced Transportation* 2021 (March): e6624130.

Ma, Wanjing, Kun An, and Hong K. Lo. 2016. "Multi-Stage Stochastic Program to Optimize Signal Timings under Coordinated Adaptive Control." *Transportation Research Part C: Emerging Technologies* 72 (November): 342–359.

Ma, Jiaman, Jeffrey Chan, Goce Ristanoski, Sutharshan Rajasegarar, and Christopher Leckie. 2019. "Bus Travel Time Prediction with Real-Time Traffic Information." *Transportation Research Part C: Emerging Technologies* 105 (August): 536–549.

Ma, Wanjing, Jinjue Li, and Chunhui Yu. 2022. "Shared-Phase-Dedicated-Lane Based Intersection Control with Mixed Traffic of Human-Driven Vehicles and Connected and Automated Vehicles." *Transportation Research Part C: Emerging Technologies* 135 (February): 103509.

Ma, Wanjing, Wei Ni, Larry Head, and Jing Zhao. 2013. "Effective Coordinated Optimization Model for Transit Priority Control Under Arterial Progression." *Transportation Research Record: Journal of the Transportation Research Board* 2356 (December): 71–83.

Ma, Wanjing, Li Zou, Kun An, Nathan H. Gartner, and Meng Wang. 2019. "A Partition-Enabled Multi-Mode Band Approach to Arterial Traffic Signal Optimization." *IEEE Transactions on Intelligent Transportation Systems* 20 (1): 313–322. https://doi.org/10.1109/TITS.2018.2815520

Mohajerpoor, Reza, Meead Saberi, and Mohsen Ramezani. 2017. "Delay Variability Optimization Using Shockwave Theory at an Undersaturated Intersection." *IFAC-PapersOnLine*, 20th IFAC World Congress 50 (1): 5289–5294. https://doi.org/10.1016/j.ifacol.2017.08.622

Su, Z. C., A. H. Chow, C. L. Fang, E. M. Liang, and R. X. Zhong. 2023. "Hierarchical Control for Stochastic Network Traffic with Reinforcement Learning." *Transportation Research Part B: Methodological* 167 (January): 196–216.

Truong, Long Tien, Graham Currie, Mark Wallace, Chris De Gruyter, and Kun An. 2019. "Coordinated Transit Signal Priority Model Considering Stochastic Bus Arrival Time." *IEEE Transactions on Intelligent Transportation Systems* 20 (4): 1269–1277. https://doi.org/10.1109/TITS.2018.2844199

Van De Weg, Goof Sterk, Hai L. Vu, Andreas Hegyi, and Serge Paul Hoogendoorn. 2019. "A Hierarchical Control Framework for Coordination of Intersection Signal Timings in All Traffic Regimes." *IEEE Transactions on Intelligent Transportation Systems* 20 (5): 1815–1827. https://doi.org/10.1109/TITS.2018.2837162

Varga, Balázs, Tamás Tettamanti, Balázs Kulcsár, and Xiaobo Qu. 2020. "Public Transport Trajectory Planning with Probabilistic Guarantees." *Transportation Research Part B: Methodological* 139 (September): 81–101. https://doi.org/10.1016/j.trb.2020.06.005

Wang, Shuling, Wei Huang, and Hong K. Lo. 2020. "Combining Shockwave Analysis and Bayesian Network for Traffic Parameter Estimation at Signalized Intersections Considering Queue Spillback." *Transportation Research Part C: Emerging Technologies* 120 (November): 102807. https://doi.org/10.1016/j.trc.2020.102807

Wu, Wei, Larry Head, Sanghuiyu Yan, and Wanjing Ma. 2018. "Development and Evaluation of Bus Lanes with Intermittent and Dynamic Priority in Connected Vehicle Environment." *Journal of Intelligent Transportation Systems* 22 (4): 301–310. https://doi.org/10.1080/15472450.2017.1313704

Xiang, Junping, and Zonghai Chen. 2016. "An Adaptive Traffic Signal Coordination Optimization Method Based on Vehicle-to-Infrastructure Communication." *Cluster Computing* 19 (3): 1503–1514. https://doi.org/10.1007/s10586-016-0620-7

Yang, Kaidi, Monica Menendez, and S. Ilgin Guler. 2019. "Implementing Transit Signal Priority in a Connected Vehicle Environment with and without Bus Stops." *Transportmetrica B: Transport Dynamics* 7 (1): 423–445. https://doi.org/10.1080/21680566.2018.1434019

Zeng, Xiaosi, Yunlong Zhang, Jian Jiao, and Kai Yin. 2021. "Route-Based Transit Signal Priority Using Connected Vehicle Technology to Promote Bus Schedule Adherence." *IEEE Transactions on Intelligent Transportation Systems* 22 (2): 1174–1184. https://doi.org/10.1109/TITS.2020.2963839

Zhou, Hongmin, H. Gene Hawkins, and Yunlong Zhang. 2017. "Arterial Signal Coordination with Uneven Double Cycling." *Transportation Research Part A: Policy and Practice* 103 (September): 409–429. https://doi.org/10.1016/j.tra.2017.07.004